The Suzaku Technical Description

Version: November 15, 2005

Announcement of Opportunity #1

Institute of Space and Astronautical Science (ISAS/JAXA)
and the
Laboratory for High Energy Astrophysics
NASA/Goddard Space Flight Center

Contents

List of Figures

List of Tables

Chapter 1

Introduction

Suzaku is the fifth in the series of Japanese astronomy satellites devoted to observations of celestial X–ray sources, following the highly successful Hakucho, Tenma, Ginga and ASCA satellites. Like ASCA, *Suzaku* is a joint Japanese-US mission, developed by the Institute of Space and Astronautical Science (part of the Japan Aerospace Exploration Agency, ISAS/JAXA) in collaboration with the National Aeronautics and Space Administration's Goddard Space Flight Center (NASA/GSFC) and many other institutions. *Suzaku* was launched on a Japanese M-V rocket on July 10, 2005 from the JAXA Uchinoura Space Center. Despite initial success, on August 8, 2005 a thermal short between the helium and neon tanks resulted in the liquid helium coolant venting to space, leaving the X–Ray Spectrometer (XRS) inoperable. However, the X–ray Imaging Spectrometer (XIS) and Hard X-ray Detector (HXD) are all working well. As a result, *Suzaku* retains its excellent X–ray sensitivity, with high throughput over a broad-band energy range of 0.2 to 600 keV. *Suzaku*'s broad bandpass, low background, and good CCD resolution makes it a unique tool capable of addressing a variety of outstanding problems in astrophysics.

Observing proposals were solicited, selected, and announced for *Suzaku* (then called Astro-E2) in 2004. However, the selection process emphasized the suitability of the XRS instrument above other instruments. Because the match between the winning proposals and the remaining capabilities of *Suzaku* is highly variable from case to case, and because the proposed and accepted integration times were often based on the feasibility of the XRS science, the international *Suzaku* project has declared the original proposal selection null and void and issued a new solicitation for proposals based solely on the HXD and the XIS capabilities.

Guest observing time on *Suzaku* will be awarded on a competitive basis and proposals will be judged on their own merits, regardless of whether they are re-submission of successful XRS proposals or not. The overall purpose of this document is to aid potential users of *Suzaku* in proposing for time during the Guest Observer (GO) phase of the mission. In particular, upon reading this document, the proposer should be able to determine whether or not *Suzaku* is best suited to conduct the investigation in question. This should be demonstrated in the proposal, preferably using simulations of the proposed observations. All proposals should clearly answer the following four questions:

1. Is *Suzaku* capable of the proposed observation?
2. Is it the best available instrument for the investigation?
3. When can *Suzaku* observe a given source?
4. How much exposure time is required to meet the scientific goals?

Chapter 2 summarizes the principal characteristics of the detectors on-board *Suzaku*. Chapter 3 covers how the satellite time will be allocated. This includes the data rights and available time for both the Science Working Group (SWG) and GOs, as well as policies regarding Targets of Opportunity (TOOs). In addition, observational constraints due to the orbit, sun angle, and the pointing accuracy are described. Finally, the proposal process is reviewed, including how to submit a proposal, how they will be evaluated, and how observations will be scheduled, performed, and the results disseminated. US proposers should note especially the NASA requirements regarding the relevance of the proposed science to NASA's mission.

Chapter 4 explains how to write a strong proposal, including a summary of what constraints must be met, and what must be included in the proposal. In most cases, existing X–ray data can be used to estimate the likely *Suzaku* count rates. Simulation tools, including **XSPEC** and **PIMMS**, will assist in this and are covered in detail with examples.

The last three chapters describe the telescopes and instruments on *Suzaku*. Chapter 5 covers the five X–ray Telescopes (XRTs) on *Suzaku*. Chapter 6 reviews the X–ray Imaging Spectrometers (XISs), four CCDs with moderate spectral resolution and a large field of view. Chapter 7 explains the operation of the Hard X–ray Detector (HXD), which extends the high energy bandpass of *Suzaku* to 600 keV.

Disclaimer:

This document was prepared using the best current knowledge of the *Suzaku* satellite by the *Suzaku* teams at ISAS/JAXA and NASA/GSFC as of November 2005. It is possible that information contained in this document may contain inadvertent errors or omissions. We welcome suggestions for corrections or clarifications. Revisions of this document will be available on the *Suzaku* Web sites listed in Appendix C.

Chapter 2

Mission Description

This chapter is a brief introduction to the satellite and its instruments, and is intended as a simplified guide for the proposer. Reading it thoroughly should provide the reader with the necessary information to understand the capabilities of the instruments at a level sufficient to prepare the feasibility section of an *Suzaku* proposal.

After launch, *Suzaku* underwent an initial checkout phase lasting approximately 4 weeks, including instrument turn-on and initial calibration, during which time the loss of liquid helium cut short XRS operations. Nonetheless, SWG science observations using the XIS and HXD began in August 2005, and will continue until March of 2006, after which Guest Observer (GO) observations will commence.

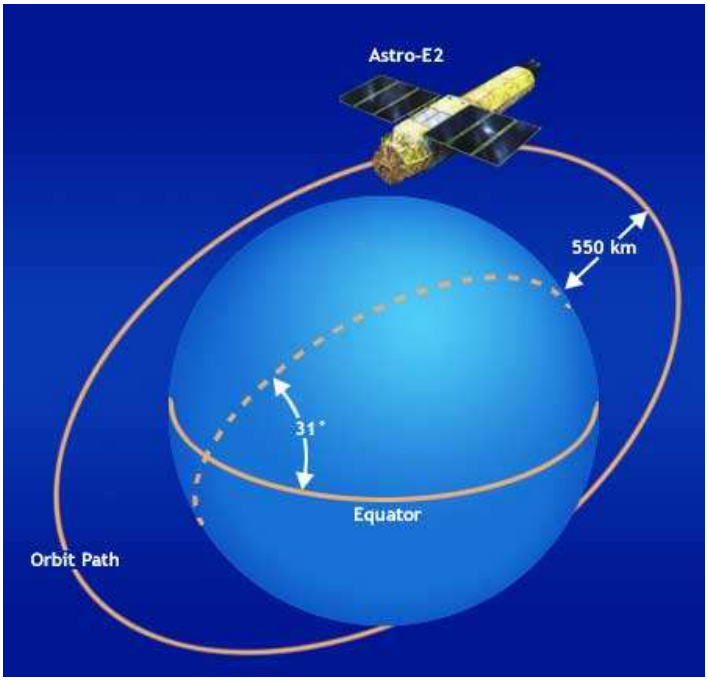

Figure 2.1: The 96 minute *Suzaku* orbit.

Suzaku is in many ways similar to ASCA in terms of orbit, pointing, and tracking capabilities. *Suzaku* uses the same station (USC) as ASCA did for uplink and downlink, although downlink at NASA DSN is not possible with Suzaku (see footnote in subsection 2.2.2). As a result, the operational constraints for *Suzaku* are also similar to those of ASCA. *Suzaku* is placed in a near-

circular orbit with an apogee of 568 km, an inclination of 31.9 degrees, and an orbital period of about 96 minutes. The maximum slew rate of the spacecraft is 6 degrees/min, and settling to the final attitude takes ~ 10 minutes, using the star trackers. The normal mode of operations will have the spacecraft pointing in a single direction for at least 1/4 day (10 ksec; but see "raster-scanning" in section 2.2.1). With this constraint, most targets will be occulted by the Earth for about one third of each orbit, but some objects near the orbital poles can be observed nearly continuously. The current projection is that the observing efficiency of the satellite will be about 43%.

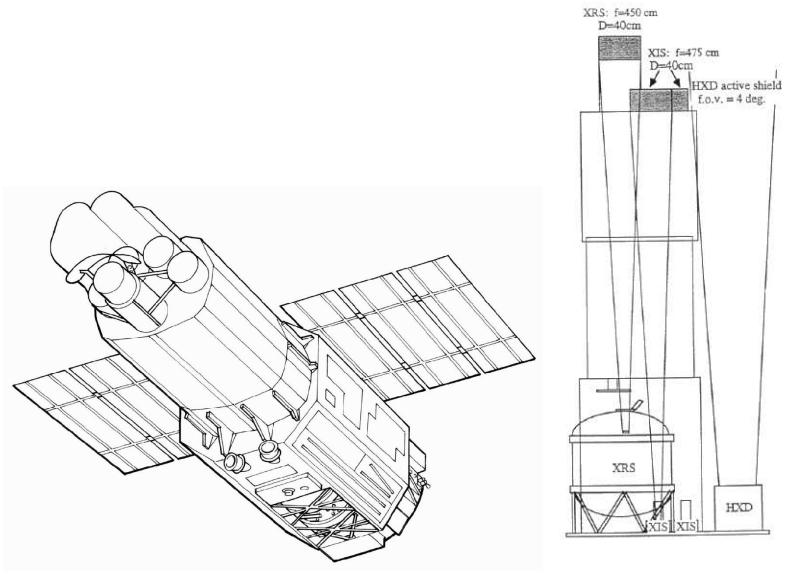

Figure 2.2: [Left] Schematic picture of the bottom of the *Suzaku* satellite. [Right] A side view of the instrument and telescopes on *Suzaku*.

2.1 A Brief Introduction to *Suzaku*

The scientific payload of *Suzaku* (Fig. 2.2) initially consisted of three distinct co-aligned scientific instruments. There are four X–ray sensitive imaging CCD cameras (X–ray Imaging Spectrometers, or XISs), three front-illuminated (FI; energy range 0.4-12 keV) and one back-illuminated (BI; energy range 0.2-12 keV), capable of moderate energy resolution. Each XIS is located in the focal plane of a dedicated X–ray telescope. The second instrument is the non-imaging, collimated Hard X–ray Detector (HXD), which extends the bandpass of the observatory to much higher energies with its 10–600 keV pointed bandpass. The X–Ray Spectrometer (XRS) is no longer operational, and will not be discussed further.

All of the instruments on *Suzaku* operate simultaneously. Each of the co-aligned XRTs features an X–ray mirror with an angular resolution (expressed as Half-Power Diameter, or HPD) of $\sim 2'$ (cf. Fig. 2.4). Figure 2.3 shows the total effective area of the XIS+XRT, which includes features due to the elemental composition of the XIS and XRT. K-shell absorption edges from the oxygen (0.54 keV) and aluminum (1.56 keV) in the blocking filters are present, as well as a number of weak M-shell features between 2–3 keV arising from the gold in the XRT.

The four XISs (cf. Fig. 6.2) are true imagers, with a large field of view ($\sim 18' \times 18'$), and moderate spectral resolution.

The HXD (cf. Fig. 7.1) is a non-imaging instrument with an effective area of $\sim 260\,\mathrm{cm}^2$, featuring

S/C	Orbit Apogee	568 km
	Orbital Period	96 minutes
	Observing Efficiency	$\sim 45\%$
XRT	Focal length	4.75 m
	Field of View	$17'$ at 1.5 keV
		$13'$ at 8 keV
	Plate scale	0.724 arcmin/mm
	Effective Area	440 cm^2 at 1.5 keV
		250 cm^2 at 8 keV
	Angular Resolution	$2'$ (HPD)
XIS	Field of View	$17.8' \times 17.8'$
	Bandpass	0.2–12 keV
	Pixel grid	1024×1024
	Pixel size	24 μm× 24 μm
	Energy Resolution	~ 130 eV at 6 keV
	Effective Area	340 cm^2 (FI), 390 cm^2 (BI) at 1.5 keV
	(incl XRT-I)	150 cm^2 (FI), 100 cm^2 (BI) at 8 keV
	Time Resolution	8 s (Normal mode), 7.8 ms (P-Sum mode)
HXD	Field of View	$4.5^\circ \times 4.5^\circ$ ($\gtrsim 100$ keV)
	Field of View	$34' \times 34'$ ($\lesssim 100$ keV)
	Bandpass	10 – 600 keV
	– PIN	10 – 60 keV
	– GSO	30 – 600 keV
	Energy Resolution (PIN)	~ 3.0 keV (FWHM)
	Energy Resolution (GSO)	$7.6/\sqrt{E_{MeV}}$ % (FWHM)
	Effective area	$\sim 160\,cm^2$ at 20 keV, $\sim 260\,cm^2$ at 100 keV
	Time Resolution	61 μs
HXD-WAM	Field of View	2π (non-pointing)
	Bandpass	50 keV – 5 MeV
	Effective Area	800 cm^2 at 100 keV / 400 cm^2 at 1 MeV
	Time Resolution	31.25 ms for GRB, 1 s for All-Sky-Monitor

Table 2.1: Overview of *Suzaku* capabilities

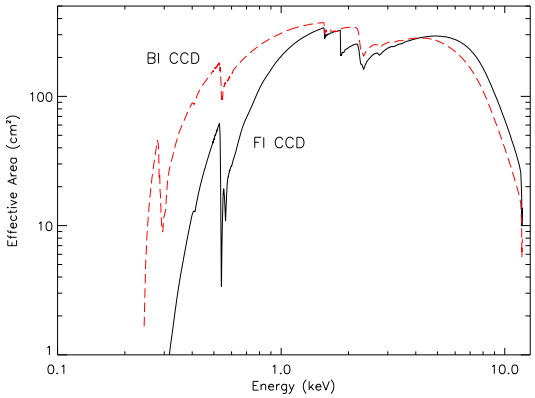

Figure 2.3: XIS Effective area of one XRT + XIS system, for both the FI and BI chips.

a compound-eye configuration and an extremely low background. It dramatically extends the bandpass of the mission with its nominal sensitivity over the 10 – 600 keV band (cf. Fig. 2.5). The HXD consists of two types of sensors: 2 mm thick silicon PIN diodes sensitive over 10 – 60 keV, and GSO crystal scintillators placed behind the PIN diodes covering 30 – 600 keV. The HXD field of view is actively collimated to $4.5^\circ \times 4.5^\circ$ by the well-shaped BGO scintillators, which, in combination with the GSO scintillators, are arranged in the so-called phoswich configuration. At energies below $\sim$ 100 keV, an additional passive collimation further reduces the field of view to $34' \times 34'$. The energy resolution is ~ 3.0 keV (FWHM) for the PIN diodes, and $7.6/\sqrt{E}$ % (FWHM) for the scintillators (where E is energy in MeV). The HXD time resolution for both sensors is 61 μs. While the HXD is intended mainly to explore the faintest hard X–ray sources, it can also tolerate very bright sources up to $\sim$ 10 Crab. The HXD also has an all-sky monitor (the Wide-band All-sky Monitor (WAM), which can detect GRB and other sources. Although observers will receive data from the WAM, it cannot be proposed for directly and has special rules regarding data rights; see Chapter 3.

Because the HXD bore-sight axis, with the highest effective area, is about 3.5 arcmin shifted from that of the XISs, *Suzaku* supports two aimpoints, XIS and HXD oriented. Users are requested to select which pointing axis is best for your observations. For the XIS, choosing the XIS aimpoint provides a $\sim$ 10% larger XIS effective area than the HXD aimpoint. Conversely for the HXD, the HXD aimpoint provides a $\sim$ 10% larger HXD effective area than the XIS aimpoint. Note that a 10% increase in effective area corresponds to a 20% increase in observing time for background dominated observations. For source dominated observations, the effect is 10%. Please take into account these effects in your observation plan.

2.2 Operational Constraints of *Suzaku*

2.2.1 Raster-scanning

While a substantial change of the spacecraft attitude (more than a few degrees) is time-consuming, small offsets can be made efficiently. Such offsets would require that no new stars need to be acquired by the star trackers, and thus are limited to $\sim 30'$. This is particularly useful in checking for point sources that in the HXD FOV but outside the XIS FOV. The minimum total time is still

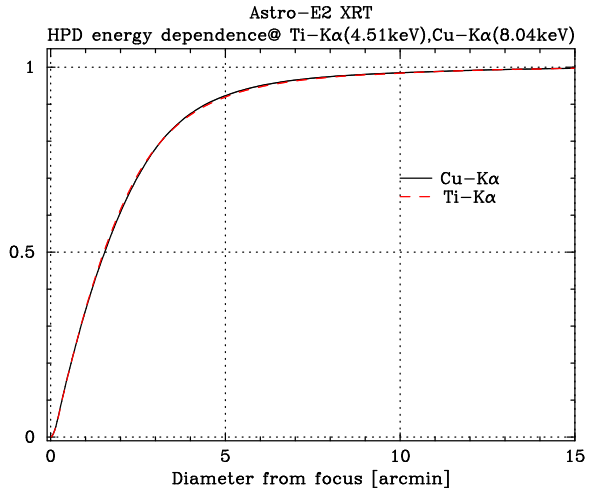

Figure 2.4: The Encircled Energy Function (EEF) showing the fractional energy within a given radius for one quadrant of the XRT-I telescopes on *Suzaku* at 4.5 and 8.0 keV.

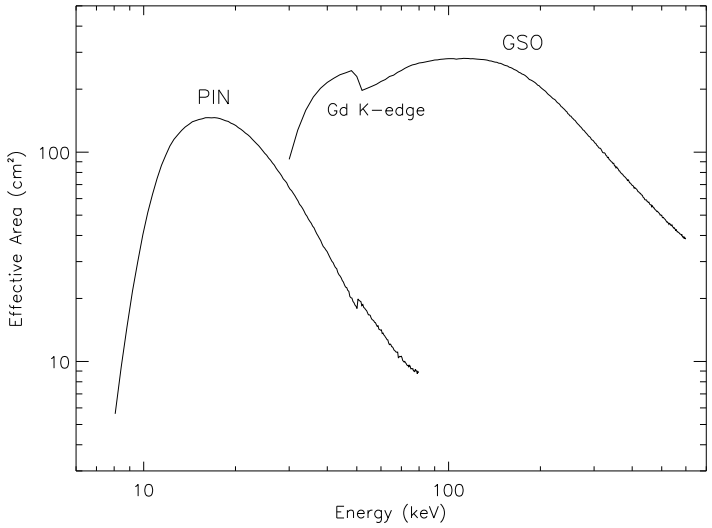

Figure 2.5: Total effective area of the HXD detectors, PIN and GSO, as a function of energy.

10 ksec, and each point in the raster scan must be observed for at least 3 ksec. Raster-scanning observations should be specified on the RPS form, with the details to be entered in the "remarks" field. If the raster-scan pattern is complex or unusual, PIs are encouraged to contact the *Suzaku* team at ISAS/JAXA or the NASA *Suzaku* GOF for assistance before submitting a proposal.

2.2.2 Telemetry rates

Suzaku carries a 6 Gbit data recorder. Data will be downlinked to USC at a rate of 4 Mbps for a total of 2 Gbits per pass, up to 5 times a day. This allows a maximum of 10 Gbits of data to be obtained per day, but fewer passes may be available to *Suzaku* as it will share the use of USC ground station with other ISAS satellites[1]. Data can be recorded at 4 different rates: Super-High (524 kbps), High (262 kbps), Medium (131 kbps), and Low (33 kbps). The recording rate will be changed frequently throughout an observation, according to a sequence that will be determined by the operations team at ISAS. This is to optimize the selection of the data rates and the usage of the data recorder, taking into account the expected count rates supplied by the proposers. Thus an accurate estimation of the count rates is important for the optimization of the mission operation. We emphasize that proposers cannot arbitrarily choose the data recording rate.

On-source data will usually be recorded at High (during contact orbits, during which the satellite passes over USC) or Medium (during remote orbits, without USC passes) data rate. The Low rate will primarily be used for times of Earth occultations and SAA passages, as the background rates in the XIS and HXD exceed their telemetry allocation limit at Low data rate. The telemetry limits for the XIS are presented in Chapter 6. The XIS data mode will be chosen for each data recording rate used to prevent telemetry saturation, based on the count rate supplied by the proposer.

2.2.3 Summary

Suzaku excels for observations such as:

- Studies of diffuse soft X-ray sources with low surface brightness: the low background, soft

[1]Unlike ASCA, NASA DSN stations will not be used, since a 4 Mbps down-link is not possible at DSN stations.

X-ray sensitivity, and near-Gaussian response of the XIS BI CCD makes such targets an excellent use of *Suzaku*.

- Observations requiring sensitivity both above and below 10 keV, especially measuring the Fe K complex simultaneously with the hard (> 10 keV) continuum.
- Rapid variability studies on 10 msec time scales. The best time resolution available on the XIS is ~ 7.8 ms, while the HXD time resolution is $\sim 61\mu$sec (see Table 2.1)

Suzaku is less appropriate for:

- Studies requiring primarily high spatial resolution. *Chandra*'s PSF is $\sim 100\times$ smaller than *Suzaku*'s, while the *XMM-Newton* PSF is $\sim 10\times$ smaller.
- Studies requiring primarily high spectral resolution. The gratings on *Chandra* and *XMM-Newton* have significantly higher resolution than the XIS.

2.3 *Suzaku* Calibration

Calibration observations for *Suzaku* started ∼4 weeks after the launch. Initial calibration observations have been completed, and now most calibration observations are performed to check long term variations. The list of all calibration targets done during Phase-1A can be found on the *Suzaku* websites listed in Appendix C.

Table 2.2 summarizes the calibration items of all scientific instruments, the current status, and their expected accuracy. These values are the 90% limits, equivalent to 1.6σ. Note that the values listed are those required from the scientific purpose and ultimate goals which are possible to be realized on the basis of the instrument design, and are not measurement results. Since the scientific instruments of *Suzaku* are very sensitive to the environment, it is inappropriate to reply on the ground data for some of the calibration items. We will add a column to the table representing the results from inflight calibration until the start of AO-1 observations (April 2006). Please regard the current values in the table as providing rough idea on the order of calibration accuracy in orbit.

Note from the XRT team — All the values about the XRT in table 2.3 are estimated from preliminary results of the flight calibrations. The XRT team will update these values as flight calibrations progress

Note from the XIS team — As this document is being written, flight data of the calibration observations are still under analysis. Some of the values in table 2.2 are based on ground calibration. Furthermore, since the XIS will suffer the radiation damage, it is very difficult to predict how the characteristics of the XIS will change in the AO1 period and how accurately the changes can be corrected. The XIS team will update these values as ground or flight calibrations progress.

Note from the HXD team — It is very difficult to estimate the background levels on the ground. The HXD team will continue study on them, and will prepare some documents on HXD background estimation until the start of AO-1 observations.

Table 2.2: Error Budgets of Scientific Instrument Calibrations

	Calibration Item	October 2005	Requirement	Goal
XRT−I/XIS	On-axis effective area [a]	∼10%	5%	5%
	Vignetting	∼50%	5%	2%
	On-axis EEF [b]	∼20%	5%	1%
	Off-axis EEF [c]	∼30%	20%	2%
	Optical axis position in XIS	∼0.5′	< 0.2′	<0.2′
	Energy scale	0.3%	0.1%	0.1%
	Energy resolution (FWHM) at 5.9 keV	5%	1%	1%
	OBF integrity	unbroken	broken/unbroken	broken/unbroken
HXD	Absolute effective area	20%	20%	5%
	Relative effective area	10%	10%	5%
	Vignetting	5%	10%	5%
	Background modeling (PIN)[d]	5%	10%	1%
	Background modeling (GSO)[d]	10%	10%	3%
	Absolute timing[e]	N/A	300 μs	100 μs
	Relative timing[e]	N/A	10^{-8}	10^{-10}
	GRB absolute timing	N/A	100 ms	15 ms

Note ··· All the values quoted are preliminary.

a: Valid in the 1–8 keV band. Calibration uncertainty may become larger outside this energy range, especially below 0.3 keV (BI chip) and above 10 keV.

b: For all integration radii from 1′-6′. No error on attitude control is included.

c: As on-axis but for all XIS f.o.v. No calibration is currently scheduled.

d: Study continues. The HXD team will prepare some documents on HXD BGD estimation for updated results by the start of AO-1 observations. Although the "Goal" will require a few years to achieve, a "tentative goal" within a year is 3% for the PIN and 5% for the GSO.

e: The requirement will be met; the HXD team will prepare the quantitative value before the start of AO-1 observations. The Crab and PSR 1509 pulses are clearly detected in the quick look analysis of calibration data.

Chapter 3

Observation Policies

The current schedule for the time allocation of the *Suzaku* mission is given in Table 3.1. For the purpose of proposal selection, we assume 37 ksec of good on-source time per day, and 360 days of operations per year. From the total of 13320 ksec, we subtract 4% of the available time as observatory time used for satellite maintenance and similar purposes, and 3% for ongoing calibration observations. Finally, 5% is earmarked as Director's Discretionary Time (DDT) for unproposed TOOs (including observations of gamma-ray bursts) and other important observations, granted at the mission director's discretion. Therefore $13320 \times 0.88 = 11722$ ksec is nominally available to the community via the proposal selection process.

The project will oversubscribe this total by 40% including category C targets whose observations are not guaranteed (see §3.4 below). If the actual observing efficiency is higher than 37 ksec per day, or if less the actual sum observatory, calibration, and director's times is less than 12%, additional C targets will be observed.

Therefore, the net observing time in the current AO available for purely Japanese proposals is 4923 ksec, while US-only proposals will occupy 4396 ksec, with an additional 1465 ksec of joint Japanese-US time. European (ESA) proposals will receive 938 ksec of observing time. Proposals from non-US, non-ESA countries will be accepted within the Japanese time up to the ESA portion.

The nationality of the PI's institution determines which agency should receive the proposal. That is, resident researchers at US institutions must submit their proposals to NASA and those at institutions in ESA member countries must submit theirs to ESA. While the ISAS/JAXA proposal process is primarily aimed at researchers resident in Japan, proposals from researchers in other (non-US, non-ESA) countries will also be considered. In addition, Co-Is from any country may be part of any proposal.

In this AO, 12.5% of the total observing time is set aside for Japan-US joint investigations. When the respective national reviews have selected the same target, the two proposals will be merged if both teams indicated their willingness to collaborate on the RPS form, and the observation will be counted against the Japan-US time. If such mergers do not take up 12.5% of total time,

Phase	Months Post-Launch	SWG	Japan (ESA)	US	Japan/US
I (SWG)	1–8	100	0 (0)	0	0
II(AO-1)	9–20	0	50 (8)	37.5	12.5

Table 3.1: The schedule for *Suzaku* and percentage of time for each group of observers. The ESA time is in parentheses as it is part of the Japanese allotment.

the remainder will be divided between separate Japanese and US investigations.

3.1 Data Rights

The data rights policy for *Suzaku* is similar to previous missions. The normal exclusive period for both SWG and GO data is one year, except that all Phase Ia SWG science data will be made available at the end of this AO.

During the GO phase, data from calibration and TOOs requested outside the proposal process (see below) will not be considered proprietary. It is also expected that some selected targets from the SWG list will be released immediately to the community, although which targets will be released is not available as of this writing. Please check the *Suzaku* websites (see Appendix C) for updates.

Data taken during spacecraft maneuvers (often called "slew data") will be proceeded and made public immediately. Maneuver data is defined as data taken when the source out of the *Suzaku* FOV, defined as being more than 1° away. Observation time, however, will not begin until the source is stable in the FOV.

3.2 Target of Opportunity (TOO) proposals

TOO proposals are allowed for *Suzaku* through the normal proposal process, although they must be ranked as category A targets (see below) to be accepted, and proposals with TOOs should not be mixed with non-TOO targets. These should only include unpredictable phenomena in a specific target (*e.g.* SS Cyg in outburst; "Triggered Observations" in *XMM-Newton* parlance), not a generic target (*e.g.* the next Galactic supernova). The triggering criteria **must** be explicit and quantifiable, and stated in detail in the proposal text; a brief summary should appear in the Remarks section of the target form. In addition, TOO proposals must provide an estimated probability of a successful trigger during the AO-1 period. It will be the PI's responsibility to notify the *Suzaku* project when the criteria are met.

The *Suzaku* project plans to set up a mechanism through which TOO observations can be requested outside the formal proposal review process. Such observations will be performed within the DDT and there will be no proprietary period for such data (see above). This mechanism will allow previously unknown objects to be observed, once a specific object is discovered.

3.3 Pointing constraints

The Solar panels on the *Suzaku* satellite are fixed. This places a restriction on the pointing direction with respect to the satellite-Sun line: the Sun angle constraint is normally 65 – 110 degrees. This means that at any given time of the year, only a swath of the sky 45 degrees wide is accessible for astronomical observations, and thus most celestial sources are available for observations for about 50 days every 6 months. If a specific observing date or a coordinated observation with other missions is required, the proposer must first determine if the observation is possible. This can be done using the "Viewing" tool on the *Suzaku* proposal website (see Appendix C). Note that a constrained observation must be ranked as Category A (see below) to be accepted.

It is anticipated that long (>1 day) observations will be the norm for *Suzaku*, based on the *Suzaku* SWG target list. In addition, a large number of short observations is an inefficient use of the satellite because of the unusable time during slews and attitude settling. The pointing is expected to be accurate to 0.3 arcmin and can be reconstructed to better than 0.2 arcmin, except

during the initial settling period of up to 10 minutes. Moreover, there is a limit on the number of slews that can be uploaded to *Suzaku*. For these reasons, a minimum exposure time of 10 ksec has been set for all proposed observations. However, raster observations over a small ($< 0.5^\circ$) area of the sky may be allowed where the individual pointings are at least 3 ksec. For such observations, the total exposure time (which must still be at least 10 ksec) and the number of separate pointings should be entered into the RPS form. Particularly complicated operations may not be feasible; please contact either the ISAS/JAXA *Suzaku* team or the NASA *Suzaku* GOF for assistance on difficult or unusual observation plans.

There are also orbital constraints upon the orientation of the projection of the XIS CCDs on the sky. Since the *Suzaku* XIS arrays are square, with calibration sources in different corners, selecting a specific roll angle is rarely significant. However, if a specific roll angle is scientifically advantageous, the proposer must first determine if it is allowed. This can be done using the MAKI tool described in §4.7. Then the required roll range can be entered on the RPS proposal form. For objects close to the ecliptic poles it is possible to arrange for any XIS orientation by scheduling observations at a specific time, but for those located close to the ecliptic, the XIS will project on the sky in a nearly fixed orientation. **Note that any roll constraint will make a proposal time critical.** Due to their increased overhead, only a fraction of the total available time can be used for constrained observations, and proposers should justify their requirements carefully.

During a pointed observation, there will be interruptions due to the location of *Suzaku* in a low Earth orbit. Normally, a target will be occulted by the Earth for ∼30 minutes every satellite orbit. In addition, *Suzaku* will pass through the South Atlantic Anomaly (SAA) during parts of 5 or 6 orbits every day. Due to the harsh radiation environment of the SAA, scientific observation is not possible during SAA passages. There are other variations in the particle background, depending primarily on the cut-off rigidity[1]. The optimal criteria to reduce times of high background while maximizes the science return is still being determined from SWG observations; please check the *Suzaku* websites (see Appendix C) for the most up-to-date suggestions.

3.4 Sequence of events after submission

After the *Suzaku* proposal deadline, there will be three independent proposal reviews for the US, Japan, and ESA proposals. Each review will create a target list from the proposed observations, ranking the accepted targets as category A, B, or C. Only category A and B targets are guaranteed to be observed. As stated above, TOOs and constrained observations are only accepted if they are in category A. Category C targets will be observed as time permits, and will not be carried over into the next AO if not observed in this AO.

Category A observations will be deemed to be complete when they have received at least 90% of the requested time with the XIS or HXD detector, as specified by the user. Category B observations are considered complete after they have been observed with the XIS or HXD for 70% of the requested time. However, these percentages are subject to change as experience warrants. Category C observations are performed on a best-effort basis.

Even though observations are scheduled to acquire roughly the approved exposure time, and ASCA experiences suggest this will usually be achieved with *Suzaku*, occasional losses of usable observation time are inevitable. Additional observations will be scheduled automatically for non-time-critical targets whose observations are considered incomplete by the project scientist at ISAS.

[1] *Suzaku* is protected from solar and cosmic-ray particles by the geomagnetic field; cut-off rigidity is an indicator of the minimum momentum required for a particle to reach a specific location, given the average geomagnetic field configuration.

In the case of time-critical observations which are incomplete or unusable, it will be the PI's responsibility to determine the best course of action.

An international merging committee will collate the three target lists and produce a single, unified list. Overlaps between US and Japanese targets will be resolved, either by merging the investigations (if both parties are willing) or by choosing one. In the latter process, the priority given by the national reviews, as well as the lengths of the accepted observations, will be considered. The final target list will be $\sim 40\%$ oversubscribed. Category A targets will have 50% of the available time, category B 40%, and category C 50%.

US PIs, or US Co-Is on foreign PI projects, may propose for funding once notified that their target has been accepted. This process is described in ROSES 2005 document; further details of this process will be made available on the NASA *Suzaku* GOF website listed in Appendix C.

Each PI will be assigned a contact scientist, either at ISAS or the NASA *Suzaku* GOF, who will work with the PI to assure the maximum science return. This will include double-checking coordinates and confirming the XIS configuration. It is important to note that once an observation has been scheduled, any delay in responding to questions from the contact scientist may result in targets being removed from the schedule. Special scheduling request and TOOs will be accommodated on a best effort basis. For simultaneous observations, the mission scheduler at ISAS, in consultation with the contact scientist, will contact the PI in advance for detailed scheduling information, and will often work directly with schedulers of other missions. For this AO, we do not have a mechanism to approve coordinated observations with *Suzaku* and another observatory through a single proposal. It is the PI's responsibility to secure observing time with other observatories, when simultaneous observations are desirable; **the *Suzaku* component of such a proposal may be approved contingent on the success of other proposals.**

Once the observation has been completed, the data will be promptly run through the processing pipeline and put into both the US and Japanese archives, initially in encrypted form. The PI will be sent the decryption key along with instructions on how to download and decrypt the data. The only exception to the one year exclusive period for GO data, in regards to the HXD Wide-band All-sky Monitor (WAM) data (see Chapter 7). The WAM is primarily used for anticoincidence shielding in the HXD, but it can also be used as an all-sky monitor, detecting solar flares, gamma-ray bursts, and other bright X-ray sources (*e.g.* Cyg X-1). All data from the WAM will be monitored by the HXD team, which will alert the GRB community to any detected bursts. In addition, the HXD team will make analysis results from WAM, such as light curves and fluences, available to the public as soon as possible. These may be used to put limits on GRBs or other events triggered by other satellites or observatories. However, the PI will receive the complete WAM data from their observation and will share data rights with the *Suzaku* team for the normal 1 year proprietary period. This unusual arrangement is due to the time-critical and non-source-specific nature of the WAM data.

With the exception of the code that converts raw binary telemetry into FITS format files, all *Suzaku* software will be written as FTOOLS and distributed through the *Suzaku* team at ISAS/JAXA and the NASA/GSFC HEASARC. This includes the tools used in the processing. All calibration files will be distributed through the HEASARC `caldb` (Calibration Database) system. This will enable users to apply any calibration updates themselves. The *Suzaku* team at ISAS and the NASA *Suzaku* GOF will provide additional FTOOLS that may be necessary or desirable in analyzing *Suzaku* data. Use of other software packages will only be supported at a lower priority level.

Chapter 4

Guide to Writing A *Suzaku* Proposal

Each *Suzaku* proposal must include at a minimum the source coordinates, exposure time, instrument configuration and expected count rates, and any observing constraints within the four page limit. The review panels will base their decision primarily upon the justification of the proposed science to be done with the data. This chapter describes how to prepare a strong proposal, including the various software tools available to assist the proposer.

4.1 Ingredients of a Successful *Suzaku* Proposal

While it is conceivable that one would wish to study a previously unknown X–ray source with *Suzaku*, a more likely scenario would involve a spectroscopy study of an object with known X–ray flux. A viable proposal should state the scientific objective of the observation and show that *Suzaku* can achieve this objective. Observations that require one or more of *Suzaku*'s unique capabilities would be especially strong canditates.

Every *Suzaku* proposal must have an estimate of the expected source count rates from the proposed target for all detectors. This rate is used both by the reviewers to evaluate the viability of the proposal and the operations team to evaluate any safety concerns. The simplest tool to use in estimating the expected XIS or HXD count rate is PIMMS. This tool is freely available as a stand-alone tool or on the Web as WebPIMMS (see Appendix C). The next level of detail is provided via simulations using XSPEC, and such simulations should provide significant insight into the expected spectrum obtained from a proposed observation. A brief guide to XSPEC simulations is given in § 4.3. In many case, this should be sufficient for a point source. There are also tools available to simulate imaging data, which may be useful for an extended source or a particularly bright source. In particular, the most powerful tool is `xissim`, which can use a FITS format image with an assumed spectral shape of the source to estimate the distribution of events in all elements of the XIS detectors.

4.2 Using PIMMS and WebPIMMS

This tool is an interactive, menu-driven program, which has an extensive HELP facility. It is also available as the web-based tool WebPIMMS. In either case, users specify the flux and spectral model with its parameters, and PIMMS/WebPIMMS returns the predicted counting rate. PIMMS/WebPIMMS can be used for a variety of other instruments, so if for instance the counting rate and spectrum of a given source observed with the ROSAT PSPC is known, it can calculate the

flux, which in turn can be used as input to estimate the expected counting rates. The limitations of the input source must be considered carefully. For example, ROSAT had no significant response to X–rays above ~ 2.4 keV, and so is not useful when estimating the HXD GSO count rate.

4.3 Using XSPEC to Simulate an Observation

Perhaps the easiest tool for simulating X–ray spectra is the XSPEC program (a part of the XANADU software package), which is designed to run on a variety of computer platforms and operating systems and is freely distributed on the NASA GSFC HEASARC Website (see Appendix C). The simulation of an XIS or HXD observation requires the current instrument redistribution matrix (the so-called .rmf file) and the energy-dependent effective area of the instrument (the so-called .arf file), both available on the Web or via anonymous FTP (see Appendix C).

The procedure for simulations is relatively simple: if the XSPEC program is installed, one should start XSPEC making sure that the proper .rmf and .arf files are accessible. Within XSPEC, one should specify the spectral model, such as hot thermal plasma or the like (via the *model* command). Specifying the model will drive XSPEC to query for the model parameters (such as temperature and abundances for an APEC collisional plasma model), as well as normalization. The key command to create a simulated spectrum is the *fakeit* command, which will query for the redistribution response (the .rmf file), and the ancillary response (the .arf file). The *fakeit* command also will request the simulated data filename, and the length of simulated observation. One can now use this file within XSPEC to determine the sensitivity of the simulated data file to changes in the model parameters.

4.3.1 Using WebSPEC to Simulate an Observation

Most of the features of XSPEC are also available as a web-based tool on the HEASARC website (see Appendix C). WebSPEC calls XSPEC behind the scenes, so all the issues described above apply here as well.

After selecting the instrument, WebSPEC allows the user to choose the spectral model, such as an absorbed collisional plasma or a power-law spectrum with an absorption component. The next page will then query for the model parameters (such as temperature and abundances for an APEC collisional plasma model), as well as normalization, exposure, upper and lower energies, and the number of bins to use in the spectral plot. WebSPEC will then create a simulated spectrum after clicking the "Show me the Spectrum" button, using the *fakeit* command. This folds the specified model through the instrument response and effective area, calculating the observed count rate and fluxes as well. WebSPEC will then allow one to download the postscript file of the spectrum, change the model parameters, or replot the data.

4.4 Examples

To show how to estimate the proper exposure, we include some simple examples of XIS and HXD observations that illustrate the process.

4.4.1 Detecting Faint Oxygen Emission from the Local Hot Bubble

The Local Hot Bubble is the proposed origin for at least some of the 1/4 keV emission seen in the ROSAT All-Sky Survey at all latitudes. Although *Suzaku* has some sensitivity at 1/4 keV, a more

profitable approach to finding this emission is to detect the OVII emission that should accompany it. In this case we need to calculate the expected count rate from the OVII and compare it to the expected background.

We first need the expected flux, based on published papers or the PI's model. In this case, we expect the surface brightness to be 0.34 ph/cm^2/s/sr, based on a number of papers. Since the XIS field of view is $18' \times 18'$, this value corresponds to a total surface brightness in one XIS of 9.3×10^{-6} ph/cm^2/s. The next question is the effective area of the XIS instruments at the line energy. OVII is in fact a complex of lines, centered around 0.57 keV. Examining the effective area plots for the XIS in Chapter 6, we see that the effective area at 0.57 keV in the BI CCD is $\sim 140\,\mathrm{cm}^2$; for the FI CCDs it is $\sim 90\,\mathrm{cm}^2$. The effective area curves for the FI and BI CCDs can also be found by loading their responses into XSPEC and using the `plot efficiency` command. *Warning:* The XIS .rmf response matrices are **not** normalized, and so must be combined with the .arf files to determine the total effective area.

With the expected flux and the effective area, we can now determine the expected count rate in the BI and FI CCDs to be 1.3 and 0.87 cts/ks. This is obviously a extremely low count rate and so the expected background is very important. The resolution of the XIS is quite good, as shown in Chapter 6, at 0.57 keV a bin of width 60 eV will contain most of the emission. The XIS background rate (see §6.7) at this energy is only 0.05 cts/s/keV in both the FI and BI detectors, so we can expect a background of 3 cts/ks. In both the FI and BI detectors the line will be below the background, but this does not intrinsically hinder detection. As will be seen below, in the HXD this is the norm rather than the exception. One aid for this observation is that the OVII line is relatively isolated in this energy range, with the exception of the nearby OVIII line. Assume we wish to detect the OVII feature with 3σ significance. Then the total count rate in the XIS-S1 (the BI CCD) in our energy band will be 4.3 cts/ks, with 3 cts/ks of background. In an N ks observation, we will measure the signal to be $1.3 \times N \pm \sqrt{4.3 \times N}$. To achieve a 3σ result, then, we need $1.3 \times N/\sqrt{4.3 \times N} > 3$, or $N > 23\,\mathrm{ks}$.

4.4.2 Detecting the hard tail of an XRB

Another common observation will be to search for faint hard X–ray tails from sources such as X–ray binaries. We describe here how to simulate such an observation, including the all-important HXD background systematics, which will dominate all such observations.

The first step is to download the latest versions of the background template files and the response files from the website listed in Appendix C. The HXD website will also describe the current best value for the systematic error in background estimation. For this AO, the HXD recommends 3% for the PIN and 5% for the GSO. Before beginning this process, the proposer should also check if contaminating sources exist in the FOV of the HXD, using existing hard X–ray source catalogs from satellite such as RXTE-ASM, INTEGRAL, and Swift.

We set up XSPEC to use these by reading the background template files as both data and background along with the response files.

```
XSPEC12>data ae_hxd_pinbkg_20051105.pha ae_hxd_gsobkg_20051105.pha

2 spectra  in use

Source File: ae_hxd_pinbkg_20051105.pha
Net count rate (cts/s) for Spectrum:1    6.689e-01 +/- 2.082e-03
```

```
 Assigned to Data Group 1 and Plot Group 1
  Noticed Channels:  1-256
  Telescope: SUZAKU Instrument: HXD  Channel Type: PI
  Exposure Time: 1.544e+05 sec
 No response loaded.

Source File: ae_hxd_gsobkg_20051105.pha
Net count rate (cts/s) for Spectrum:2    3.539e+01 +/- 2.571e-02
 Assigned to Data Group 1 and Plot Group 2
  Noticed Channels:  1-512
  Telescope: SUZAKU Instrument: HXD  Channel Type: PI
  Exposure Time: 5.354e+04 sec
 No response loaded.

***Warning!  One or more spectra are missing responses,
               and are not suitable for fit.
XSPEC12>back ae_hxd_pinbkg_20051105.pha ae_hxd_gsobkg_20051105.pha
***Warning!  One or more spectra are missing responses,
               and are not suitable for fit.
Net count rate (cts/s) for Spectrum:1    -0.000e+00 +/- 2.944e-03 (-0.0  % total )
Net count rate (cts/s) for Spectrum:2    -0.000e+00 +/- 3.636e-02 (-0.0  % total )
XSPEC12>resp ae_hxd_pinhxnom_20051104.rsp ae_hxd_gso_20051019.rsp
Response successfully loaded.
Response successfully loaded.
```

Now we assume a spectrum for our source; here, we use a Crab-like spectrum (photon index 2.1) with a 10 mCrab flux. This can be set up in XSPEC via the following commands:

```
XSPEC12>model powerlaw

Input parameter value, delta, min, bot, top, and max values for ...
              1       0.01         -3         -2          9         10
powerlaw:PhoIndex>2.1
              1       0.01          0          0      1e+24      1e+24
powerlaw:norm>0.08

========================================================================
Model powerlaw<1> Source No.: 1   Active/Off
Model Model Component  Parameter  Unit     Value
 par  comp
   1    1   powerlaw   PhoIndex            2.10000      +/-  0.0
   2    1   powerlaw   norm                8.00000E-02  +/-  0.0
------------------------------------------------------------------------


 Chi-Squared =       39667.42 using 768 PHA bins.
 Reduced chi-squared =       51.78514 for    766 degrees of freedom
 Null hypothesis probability =   0.000000e+00
 Valid fit does not exist.
```

Now we can create fake PIN and GSO data with the "fakeit" command. The result will be simulated spectral files which include the instrumental background, effective area, and resolution.

```
XSPEC12>fakeit
 Use counting statistics in creating fake data? (y):
 Input optional fake file prefix:
 Fake data file name (ae_hxd_pinbkg_20051105.fak): pin_10mCrab_100ks.fak
 Exposure time, correction norm (154410., 1.00000): 1e+5
 Fake data file name (ae_hxd_gsobkg_20051105.fak): gso_10mCrab_100ks.fak
 Exposure time, correction norm (53537.7, 1.00000): 1e+5

No ARF will be applied to fake spectrum #1

No ARF will be applied to fake spectrum #2
```

We have now created our 'faked' spectral files, named `pin_10mCrab_100ks.fak` and `gso_10mCrab_100ks.fak`. Now we fit these datasets with the same Crab-like model. We will use three different background spectral models–low, medium, and high–which vary by as much as 3% for the PIN and 5% for the GSO. This takes into account the fact that the "true" background will likely vary within these limits. One item of note is that we do **not** use the "faked" background files afterwards which were also created by the fakeit command. That process assumes that the background is obtained together with the actual observation, *e.g.* using the outer region of the CCD image. In an HXD observation, this is not the case. The background is generated by modeling from the database, and users should use the template background throughout the simulation and also the future analysis.

We load the background files twice, once as background and once as a correction file ("corfile") which will allow us to easily vary the total background within XSPEC.

```
XSPEC>back ae_hxd_pinbkg_20051105.pha ae_hxd_gsobkg_20051105.pha

XSPEC>corfile ae_hxd_pinbkg_20051105.pha ae_hxd_gsobkg_20051105.pha
```

All the necessary data files are now loaded, and we now experiment with different background levels, set by the value of "cornorm". A value of 0 gives the "normal" background, for example, and 0.05 increases it by 5%.

```
XSPEC>cornorm 0.0 0.0
XSPEC>ignore 1:**-8.0 2:**-30.0 600.0-**
XSPEC>setplot energy
XSPEC>setplot rebin 3 30
XSPEC>plot ldata
XSPEC>fit
XSPEC>plot ldata res
```

Now we check that the same source signal would be detectable with a high background–3% for the PIN and 5% for the GSO.

```
XSPEC>cornorm 0.03 0.05
XSPEC>plot ldata
```

```
XSPEC>ignore 2:30.0-600.0
XSPEC>fit
XSPEC>plot ldata data
```

From the initial `plot ldata` command it is seen that in this case the signal is undetectable at all in the GSO band, and so the entire GSO band is ignored.

Finally, we check the source signal using low backgrounds.

```
XSPEC>cornorm 1 -0.03 -0.05
XSPEC>plot ldata
XSPEC>fit
XSPEC>plot ldata data
```

By comparing the different fit results from these different runs, the total expected error in the slope and normalization can be estimated.

4.4.3 Measuring the Reflection Component of an AGN

Our goal is to measure the contribution reflected X–rays make to the X–ray spectrum of an AGN. The reflection occurs primarily with harder X–rays, so the HXD is the primary instrument and could be used without the XIS. However, measuring the continuum over a broad range will significantly reduce the errors (both systematic and statistical) in the result. In this example a moderately-absorbed Seyfert 2 simulation will be performed.

We begin be reading into XSPEC the XIS response and HXD background and response files we will need. These can be found on the *Suzaku* proposal website; see Appendix C. XIS-S1 is the BI chip and XIS-S2 is used to represent all three FI chips.

```
XSPEC12>data ae_xi1_back.pha ae_xi2_back.pha
XSPEC12>data 3 ae_hxd_pinbkg_20051105.pha ae_hxd_gsobkg_20051105.pha

XSPEC12>back 3 ae_hxd_pinbkg_20051105.pha ae_hxd_gsobkg_20051105.pha

XSPEC12>resp ae_xi1_20051103.rmf ae_xi2_20051102.rmf
XSPEC12>arf ae_xi1_onaxis_20050916.arf ae_xi2_onaxis_20050916.arf
XSPEC12>resp 3 ae_hxd_pinxinom_20051104.rsp ae_hxd_gso_20051019.rsp
```

Next we set up the model we want.

```
XSPEC12>model constant*phabs( pexrav + gaussian )

Input parameter value, delta, min, bot, top, and max values for ...
              1       0.01          0          0      1e+10      1e+10
constant:factor>1 -1
              1      0.001          0          0     100000      1e+06
phabs:nH>50
              2       0.01        -10         -9          9         10
pexrav:PhoIndex>1.8
            100         10          1          1      1e+06      1e+06
pexrav:foldE>100.
```

```
              0       0.01          0          0      1e+06      1e+06
pexrav:rel_refl>1
              0      -0.01          0          0         10         10
pexrav:redshift>
              1      -0.01          0          0      1e+06      1e+06
pexrav:abund>
              1      -0.01          0          0      1e+06      1e+06
pexrav:Fe_abund>
           0.45      -0.01       0.05       0.05       0.95       0.95
pexrav:cosIncl>
              1       0.01          0          0      1e+24      1e+24
pexrav:norm>
            6.5       0.05          0          0      1e+06      1e+06
gaussian:LineE>6.4
            0.1       0.05          0          0         10         20
gaussian:Sigma>0.01
              1       0.01          0          0      1e+24      1e+24
gaussian:norm>

========================================================================
Model constant<1>*phabs<2>(pexrav<3> + gaussian<4>) Source No.: 1   Active/On
Model Model Component  Parameter  Unit     Value
 par  comp
   1    1   constant   factor             1.00000      frozen
   2    2   phabs      nH         10^22   50.0000      +/-  0.0
   3    3   pexrav     PhoIndex           1.80000      +/-  0.0
   4    3   pexrav     foldE      keV     100.000      +/-  0.0
   5    3   pexrav     rel_refl           1.00000      +/-  0.0
   6    3   pexrav     redshift           0.0          frozen
   7    3   pexrav     abund              1.00000      frozen
   8    3   pexrav     Fe_abund           1.00000      frozen
   9    3   pexrav     cosIncl            0.450000     frozen
  10    3   pexrav     norm               1.00000      +/-  0.0
  11    4   gaussian   LineE      keV     6.40000      +/-  0.0
  12    4   gaussian   Sigma      keV     1.00000E-02  +/-  0.0
  13    4   gaussian   norm               1.00000      +/-  0.0
------------------------------------------------------------------------

Compton reflection from neutral medium.
See help for details.
If you use results of this model in a paper,
please refer to Magdziarz & Zdziarski 1995 MNRAS, 273, 837
Questions: Andrzej Zdziarski, aaz@camk.edu.pl

 Chi-Squared =   4.182172e+11 using 2816 PHA bins.
 Reduced chi-squared =   1.489377e+08 for   2808 degrees of freedom
 Null hypothesis probability =   0.000000e+00
 Valid fit does not exist.
```

Next we need to adjust the normalization of the continuum and Fe-K line. Here we assume our

source has a F(15-100 keV) = 5e-11. The XSPEC command:

```
XSPEC>flux 15 100
 No overlap between matrix range  (          0.2,          12 )
and the requested range (           15,         100 )
 Upper range bound          100 reset by matrix bound to       96.375
 Spectrum Number: 3
 Model Flux   0.11484 photons (5.9099e-09 ergs/cm^2/s) range (15.000 - 96.375 keV)
 Spectrum Number: 4
 Model Flux   0.11562 photons (5.9989e-09 ergs/cm^2/s) range (15.000 - 100.00 keV)
```

shows that the current flux is 6e-9. To make the model match our desired total flux, we need to change the normalization to 8.3e-3 via the command: `XSPEC> new 10 8.3e-3`

To find the correct normalization for a Fe K Gaussian with equivalent width 500 eV, we use the XSPEC eqwidth command:

```
XSPEC>eqwidth 4

Data group number: 1
Additive group equiv width for Component 4:  3274.28 keV
```

The correct normalization, therefore, is 1.53e-4. We set this value and then save the model for future use:

```
XSPEC>new 13 1.53e-4
XSPEC>save model pexrav_100kev_fek_500ev_5e-11_model.xcm
```

Now run the XSPEC "fakeit" command, with the FI CCD simulation having three times the exposure of the other instruments:

```
XSPEC12>fakeit
 Use counting statistics in creating fake data? (y):
 Input optional fake file prefix:
 Fake data file name (ae_xi1_back.fak): pexrav_100kev_fek_500ev_BI_100ks.fak
 Exposure time, correction norm (32245.7, 1.00000): 1e5
 Fake data file name (ae_xi2_back.fak): pexrav_100kev_fek_500ev_FI_300ks.fak
 Exposure time, correction norm (32245.7, 1.00000): 3e5
 Fake data file name (ae_hxd_pinbkg_20051105.fak): pexrav_100kev_fek_500ev_pin_100ks.fak
 Exposure time, correction norm (154410., 1.00000): 1e5
 Fake data file name (ae_hxd_gsobkg_20051105.fak): pexrav_100kev_fek_500ev_gso_100ks.fak
 Exposure time, correction norm (53537.7, 1.00000): 1e5

No ARF will be applied to fake spectrum #3

No ARF will be applied to fake spectrum #4
```

As with the last example we do not use the HXD backgrounds generated by fakeit but use the standard backgrounds also read in as correction files

```
XSPEC12>back 3 ae_hxd_pinbkg_20051105.pha ae_hxd_gsobkg_20051105.pha
XSPEC12>corf 3 ae_hxd_pinbkg_20051105.pha ae_hxd_gsobkg_20051105.pha
XSPEC12>corn 3-4 0.
```

Ignore some channels, plot the data to see where data quality drops off, then ignore some more channels

```
XSPEC12>ignore 1:0.0-0.3 2:0.0-0.4 3:0.0-10.0 4:0.0-30.0
XSPEC12>setplot energy
XSPEC12>setplot rebin 5 100
XSPEC12>plot ldata
XSPEC12>ignore 1:0.-2. 10.-** 2:0.-2. 11.-**
XSPEC12>ignore 3:50.-** 4:100.-**
```

Try increasing the HXD background by its uncertainty to see whether the GSO data is worth using

```
XSPEC12>corn 3 0.03
XSPEC12>corn 4 0.05
XSPEC12>plot ldata
```

Clearly we won't get a detection with the GSO within the background systematics so remove this dataset from consideration.

```
XSPEC12>data 4 none
```

We can now fit and determine the uncertainties on the reflection parameters. This should be done by using the error command on the relevant parameters to get the statistical uncertainties then repeat with all three possible normalizations of the PIN background to get the systematic uncertainties.

One other source of systematic uncertainty is the relative normalization of the instrument effective areas. This is still being calibrated but a conservative assumption would be to assume a 5% uncertainty. This can be included in the modelling by reading the three datasets of interest in as separate data groups.

```
XSPEC12>data 1:1 pexrav_100kev_fek_500ev_BI_100ks.fak
XSPEC12>data 2:2 pexrav_100kev_fek_500ev_FI_300ks.fak
XSPEC12>data 3:3 pexrav_100kev_fek_500ev_pin_100ks.fak
XSPEC12>back 3 ae_hxd_pinbkg_20051105.pha
XSPEC12>corf 3 ae_hxd_pinbkg_20051105.pha
XSPEC12>corn 3 0.
XSPEC12>ignore 1:0.-2. 10.-** 2:0.-2. 11.-** 3:0.-10. 50.-**

XSPEC> setplot energy
XSPEC> setplot rebin 5 100
XSPEC> ignore 1:11.-**
XSPEC> ignore 2:10.-**
XSPEC> ignore 3:50.-**
XSPEC> ignore 4:100.-**
```

Now set the "const" values for data sets 2 and 3 to be constrained to vary from 0.95 to 1.05.

```
XSPEC12>newpar 14 1.0 0.1 0.95 0.95 1.05 1.05
XSPEC12>newpar 27 1.0 0.1 0.95 0.95 1.05 1.05
```

and determine errors as before.

4.5 XISSIM

`xissim` is a *Suzaku* XIS event simulator, based on the tool `xrssim`. It reads a FITS format photon list file, traces photon paths in the telescope (via ray-tracing), and outputs a simulated XIS event file. XRT thermal shield transmission and XIS detection efficiency are taken into account if requested. Each record of the photon list file describes the celestial positions, arrival time, and energy of the input photon. The `mkphlist` ftool can create such photon list files from FITS images (e.g., ROSAT HRI or *Chandra* images) and spectral models (which may be created in XSPEC). The `xissim` output event file may be analyzed just like a real data, using standard analysis tools such as `xselect`.

At the time of this writing, `xissim` is not yet ready for release. Please check the *Suzaku* Tools web page listed in Appendix C for more information about the status of `xissim`.

4.6 Using Viewing

One of the first tasks in preparing a proposal is determining when and for how long a target can be observed. This can be easily done with Viewing, a simple Web-based interactive tool (see Appendix C) that can determine visibility for many different satellites. To use Viewing, simply enter the target name or coordinates, and select the satellite. Viewing will return all the available dates when that target is observable.

4.7 Using MAKI

MAKI is another Web-based interactive tool (see Appendix C) that can determine the orientation of the XIS CCDs on the sky as a function of the observation epoch within the visibility window of the target. For *Suzaku*, the orientation of the solar panels with respect to the spacecraft is fixed, and at the same time, the range of the angles between the vector normal to the solar panels and the vector pointing to the Sun is restricted, which in turn restricts the roll angle of the spacecraft.

When using the tool, general instructions are available via the "Help" button. section. To check the visibility and available roll angles for a target, first load an image. This can be done with either an existing FITS image, or by entering the RA and Declination of the source and clicking the "New Graph" button. This creates an image upon which the *Suzaku* XIS field of view (FOV) will be shown.

The "Mission and Roll Selector" (in the upper right of the display) allows different instruments from different missions to be selected. Then the FOV will appear on your image. This can be rotated using the "Roll angle" slider bar.

4.8 Guide to Using the RPS

RPS, or the Remote Proposal Submission tool, must be used to enter the basic proposal data into the ISAS/JAXA, HEASARC, or ESA database. Proposers should make sure they use the appropriate RPS, since they are multiple reviews. See Appendix C for the list of RPS websites and addresses. Two versions of RPS are available: a character-oriented version, where the user submits all the required information via e-mail, or a Web-oriented version.

One aspect of RPS that is not immediately obvious is how to specify the time-constrained observations. For instance, a need for such an observation may arise for a study of a spectrum of a binary system in a particular orbital phase. If some particular aspect of the observation cannot be clearly specified in the RPS form, the user should detail it in the "comments" field of the RPS form and/or contact either the *Suzaku* team at ISAS/JAXA or the NASA *Suzaku* GOF before submitting.

4.9 Checklist

A successful *Suzaku* proposal, from a technical point of view, must include the following elements:

Coordinates: The PI is responsible for supplying the correct J2000 coordinates. For extended sources, specify single FOVs (coordinates for the center of XIS or the HXD) or rastering parameters (a schematic drawing overlaid on images would be the least ambiguous; equivalent textual descriptions are acceptable).

XIS Count rate and exposure time: Explain how they were calculated (for a highly variable source, added explanation — such as "excluding any bursts" — would be helpful).

HXD Count rate and exposure time: If the source is not expected to be a hard X–ray source, this can be set to 0.0 since only the source counts are to be included.

Aimpoint – XIS or HXD : The HXD and XIS aimpoints differ by $3.5'$. To get the full effective area for a given instrument, the instrument-specific aimpoint must be chosen (the HXD aimpoint is at (DETX,DETY)=(-3.5′, 0) on the XIS image). The reduction in effective area for the non-selected instrument is $\sim 10\%$.

Observing constraints, if any: These include monitoring, coordinated, phase-dependent, and roll-dependent; TOOs are allowed, but the triggering criteria and the probability of triggering must be spelled out in text, and summarized in target remarks.

Note that the GOs are welcome to propose for targets already approved for the SWG time (see the Announcement of Opportunity). However, in the interest of maximizing the scientific return from *Suzaku*, the proposal must explain why the already-approved observation does not meet their scientific objectives. Valid reasons include a much longer exposure time; incompatible time constraints; different positions within an extended source.

We note also that the XISs are also subject to count rate limitations, because of possible multiple events in an XIS pixel within one frame (see § 6.6). This is much less of a problem than with the ACIS aboard *Chandra*, as *Chandra*'s mirror focuses the X–ray flux into a region of a CCD that is orders of magnitude smaller. The rule of thumb is that the XIS can tolerate a point source with a count rate up to ~ 40 cts s^{-1} per CCD with essentially no loss of counts or resolution. For brighter sources, these limitations can be reduced via a variety of XIS modes, such as the use of a sub-array of the XIS, as discussed in § 6.5.

Finally, it is important to remember that because HXD is a non-imaging detector, contaminating sources in the field of view can significantly affect your results. The HXD field of view is defined by a collimator with a square opening. The FWHM of the field of view is $34.4' \times 34.4'$ below ~ 100 keV and $4.6^{\circ} \times 4.6^{\circ}$ above ~ 100 keV. Considering that twice the FWHM value is required to completely eliminate the contamination in a collimator-type detector, and the source may happen to be located at the diagonal of the square, nearby bright sources within a radius of $50'$ and 6.5° from the aim point can contaminate the data in the energy band below and above ~ 100 keV, respectively. If you specify the roll-angle to avoid the source, the limit will be reduced to $\sim 35'$ and $\sim 4.6^{\circ}$, respectively. It is the proposer's responsibility to show that any source with a flux level comparable to or brighter than that of your interest does not exist within these ranges. The proposer can check this in the minimum level by using the hard X-ray source catalogs from such satellites as RXTE-ASM, INTEGRAL, and Swift amongst others.

4.10 Additional Requirements for US Proposers

There are three additional NASA-specific proposal rules that must be followed by US-based proposers:

1. A "Notice of Intent" (NOI) should be submitted to the Web address listed in the official announcement (see Appendix C) by December 2, 2005. US based proposers are **strongly encouraged** to submit notices of intent (NoI) through the NSPIRES system for two reasons. First, NOI submission uses the same NSPIRES system as used in the submission of NASA cover pages, which is compulsory. Submitting a NOI will ensure that the proposers are familiar with this system and that all co-Is are registered users of the NSPIRES system. Second, NOI submission facilitates the planning of the peer review, which has a very tight schedule due to the unusual circumstances of this solicitation.

2. A NASA Cover Page which includes a proposal and budget summary **must** be generated, using the Web form listed in §C. The cover page requires some budget information, and as noted in the official NASA announcement, a placeholder value of $1 should be used since budget information is not required until Stage 2. After submitting the cover page, a copy should be printed and saved for use in the Stage 2 budget process.

3. As described in the NRA, the NASA Office of Space Science **requires** all proposals to demonstrate their relationship to NASA Goals and Research Focus Areas (RFAs). Therefore, each proposal should include a sentence stating its specific relevence to one of the RFAs given in Table 1 of the Summary of Solicitation. In particular, *Suzaku* science will often address the science themes in the "Astronomical Search for Origins" and the "Structure and Evolution of the Universe."

Chapter 5

X–Ray Telescopes (XRTs)

Suzaku has five light-weight thin-foil X–Ray Telescopes (XRTs). The XRTs have been developed jointly by NASA/GSFC, Nagoya University, Tokyo Metropolitan University, and ISAS/JAXA. These are grazing-incidence reflective optics consisting of compactly nested, thin conical elements. Because of the reflectors' small thickness, they permit high density nesting and thus provide large collecting efficiency with a moderate imaging capability in the energy range of 0.2-12 keV, all accomplished in telescope units under 20 kg each.

Four XRTs onboard *Suzaku* (XRT-I) are used on the XIS, and the other XRT (XRT-S) is for the XRS. XRT-S is no more functional. The XRTs are arranged on the Extensible Optical Bench (EOB) on the spacecraft in the manner shown in Figure 5.1. The external dimensions of the 4 XRT-Is, however, are the same (See Table 5.1, which also includes a comparison with the ASCA telescopes).

The angular resolutions of the XRTs range from $1.8'$ to $2.3'$, expressed in terms of half-power diameter, which is the diameter within which half of the focused X–ray is enclosed. The angular resolution does not significantly depend on the energy of the incident X–ray in the energy range of *Suzaku*, 0.2-12 keV. The effective areas are typically 440 cm^2 at 1.5 keV and 250 cm^2 at 8 keV. The focal lengths are 4.75 m for the XRT-I. Individual XRT quadrants have their component focal lengths deviated from the design values by a few cm. The optical axes of the quadrants of each XRT are aligned within $2'$ from the mechanical axis. The field of view for XRT-Is is about $17'$ at

	Suzaku XRT-I	ASCA
Number of telescopes	4	4
Focal length	4.75 m	3.5 m
Inner Diameter	118 mm	120 mm
Outer Diameter	399 mm	345 mm
Height	279 mm	220 mm
Mass/Telescope	19.5 kg	9.8 kg
Number of nested shells	175	120
Reflectors/Telescope	1400	960
Geometric area/Telescope	873 cm^2	558 cm^2
Reflecting surface	Gold	Gold
Substrate material	Aluminum	Aluminum
Substrate thickness	155 μm	127 μm
Reflector slant height	101.6 mm	101.6 mm

Table 5.1: Telescope Dimensions and Parameters of XRT-I

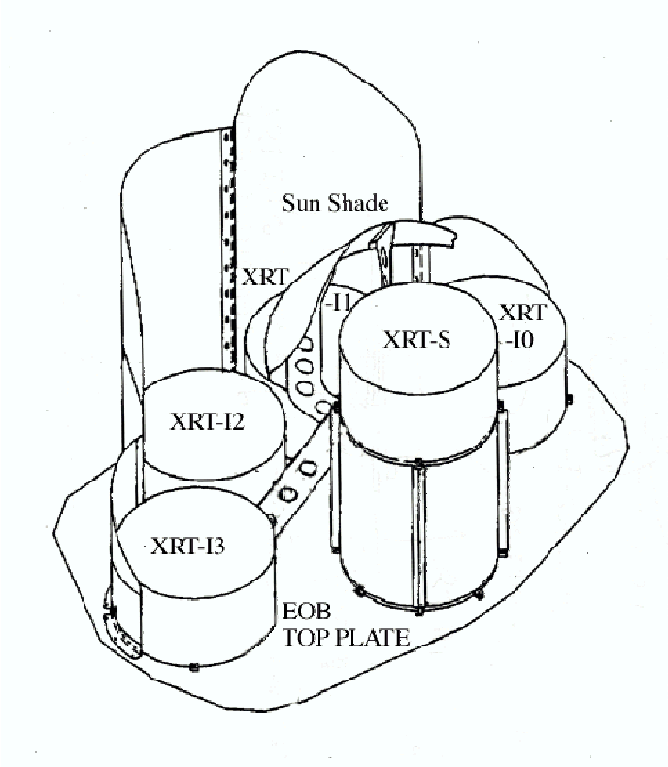

Figure 5.1: Layout of the XRTs on the *Suzaku* spacecraft.

1.5 keV and 13′ at 8 keV. (see also Table 2.1)

5.1 Basic Components of XRT

The *Suzaku* X–Ray Telescopes (XRTs) consist of closely nested thin-foil reflectors, reflecting X–ray at small grazing angles. An XRT is a cylindrical structure, having the following layered components: 1. a thermal shield at the entrance aperture to help maintain a uniform temperature; 2. a pre-collimator mounted on metal rings for stray light elimination; 3. a primary stage for the first X–ray reflection; 4. a secondary stage for the second X–ray reflection; 5. a base ring for structural integrity and interface with the EOB of the spacecraft. All these components, except the base rings, are constructed in 90° segments. Four of these quadrants are coupled together by interconnect-couplers and also by the top and base rings (Figure 5.2). The telescope housings are made of aluminum for an optimal strength to mass ratio. Each reflector consists of a substrate also made of aluminum and an epoxy layer that couples the reflecting gold surface to the substrate.

Including the alignment bars, collimating pieces, screws and washers, couplers, retaining plates, housing panels and rings, each XRT-I consists of over 4112 mechanically separated parts. In total, nearly 7000 qualified reflectors were used and over 1 million cm^2 of gold surface was coated.

5.1.1 Reflectors

In shape, each reflector is a 90° segment of a section of a cone. The cone angle is designed to be the angle of on-axis incidence for the primary stage and 3 times that for the secondary stage. They are 101.6 mm in slant length and with radii extending approximately from 60 mm at the inner part to 200 mm at the outer part. The reflectors are nominally 178 μm in thickness. All reflectors are

Figure 5.2: A Suzaku X–Ray Telescope

positioned with grooved alignment bars, which hold the foils at their circular edges. There are 13 alignment bars at each face of each quadrant, separated at approximately 6.4° apart.

To properly reflect and focus X–ray at grazing incidence, the precision of the reflector figure and the smoothness of the reflector surface are important aspects. Since polishing of thin reflectors is both impractical and expensive, reflectors in *Suzaku* XRTs acquire their surface smoothness by a replication technique and their shape by thermo-forming of aluminum. In the replication method, metallic gold is deposited on extrusion glass mandrel ("replication mandrel"), of which the surface has sub-nanometer smoothness over a wide spatial frequency, and the substrate is subsequently bonded with the metallic film with a layer of epoxy. After the epoxy is hardened, the substrate-epoxy-gold film composite can be removed from the glass mandrel and the replica acquires the smoothness of the glass. The replica typically has ∼0.5 nm rms roughness in the mm or smaller spatial scale, which is sufficient for excellent reflectivity at incident angle less than the critical angle. The *Suzaku* XRTs are designed with on-axis reflection at less than critical angle, which is approximately inversely proportional to X–ray energy.

In the thermo-forming of the substrate, pre-cut, mechanically rolled aluminum foils are pressed onto a precisely shaped "forming mandrel", which is not the same as the replication mandrel. The combination is then heated until the aluminum softened. The aluminum foils acquire the figure of the properly shaped mandrel after cooling and release of pressure. In the *Suzaku* XRTs, the conical approximation of the Wolter-I type geometry is used. This approximation fundamentally limits the angle resolution achievable. More significantly, the combination of the figure error in the replication mandrels and the imperfection in the thermo-forming process (to about 4 micrometers in the low frequency components of the figure error in the axial direction) limits the angular resolution to about 1 minute of arc.

	XRT-I
Number of Collimators	4
Height	32 mm
Blade Substrate	Aluminum
Blade Thickness	120 μm
Blade Height	22 mm
Height from Blade Top to Reflector Top	30 mm
Number of nested shells	175
Blade/Telescope	700
Mass/Collimator	2.7 kg

Table 5.2: Design Parameters for Pre-collimator

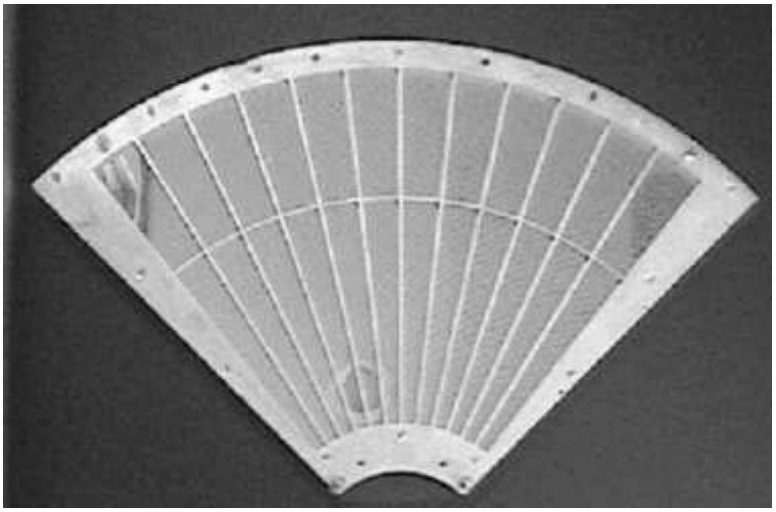

Figure 5.3: A thermal shield.

5.1.2 Pre-collimator

The pre-collimator, which blocks off stray light that otherwise would enter the detector at a larger angle than intended, consists of concentrically nested aluminum foils similar to that of the reflector substrates. They are shorter, 22 mm in length, and thinner, 120 micrometers in thickness. They are positioned in a fashion similar to that of the reflectors, by 13 grooved aluminum plates at each circular edge of the pieces. They are installed on top of their respective primary reflectors along the axial direction. Due to their smaller thickness, they do not significantly reduce the entrance aperture in that direction more than the reflectors already do. Pre-collimator foils do not have reflective surfaces (neither front nor back). The relevant dimensions are listed in Table 5.2.

5.1.3 Thermal Shields

The *Suzaku* XRTs are designed to function in a thermal environment of 20$\pm$7.5°C. The reflectors, due to its composite nature and thus its mismatch in coefficients of thermal expansion, suffer from thermal distortion that degrades the angular resolution of the telescopes in temperature outside this range. Thermal gradient also distorts the telescope in a larger scale. Even though sun shields and other heating elements on the spacecraft help in maintaining a reasonable thermal environment, thermal shields are integrated on top of the pre-collimator stage to provide the needed thermal control.

5.2 XRT-I Performance in Orbit

5.2.1 Focal Positions and Angular Resolutions

A point-like source MCG−6−30-15 were observed at the XIS aimpoint during August 17-18. We subtracted a constant value, evaluated from source-free corner regions as a background, from all the pixels. We used the data taken only during the star-tracker calibration is on. In Fig. 5.4, we show the images and the point spread functions (PSFs) of all the XRT-I+XIS modules. The preliminary HPD, with a typical statistical error of $\sim 0'.1$, ranges from $1'.8 \sim 2'.3$.

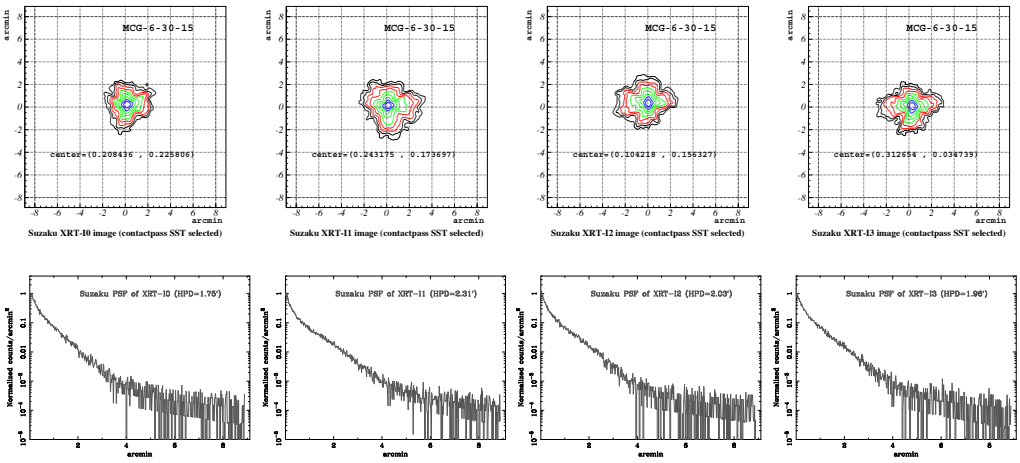

Figure 5.4: Images and PSFs are shown in the upper, middle, and lower panels for the XRT-I0 through XRT-I3 from left to right. In each image drawn are ten contours in logarithmic spacing with the outermost contour being 1% surface brightness of the peak. The position of the maximum surface brightness is written as a caption in each panel in a unit of arcmin. Its typical error is $\pm 0'.1$. Each PSF is normalized by the number of total photons collected over the entire XIS aperture.

Figure 5.5 shows the focal position of the XRT-Is, that the source is focused when the satellite points at the XIS aimpoint. The focal positions locate roughly within $0'.5$ from the detector center with an deviation of $\sim 0'.3$. This implies that the fields of view of the XIS coinsides each other within $\sim 0'.3$.

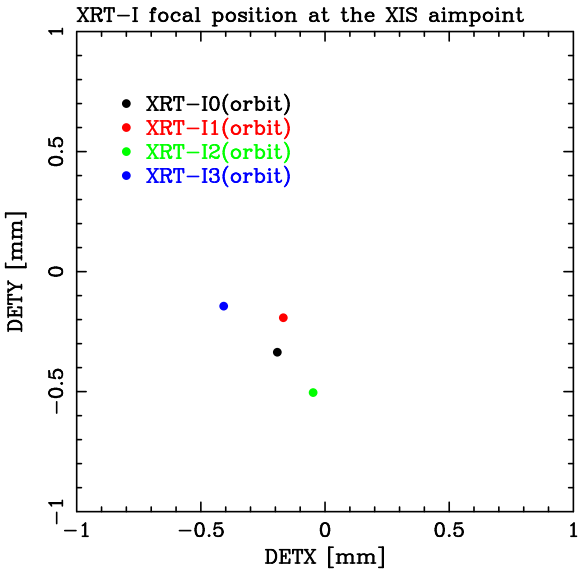

Figure 5.5: Focal positions at the XISs when the satellite points MCG−6−30-15 at the XIS aimpoint.

5.2.2 Optical Axes, Effective Area and Vignetting Functions

A series of offset observations of the Crab observations were carried out in August and Septemper at various off-axis angles of $0'$, $3.'5$, $7'$. The intensity of the Crab nebula is evaluated for each pointing and for each XIS module separately. By finding the maximum throughput angle, we also have obtained a direction of the optical axis of each telescope. The result is shown in Fig. 5.6 The optical axes locate roughly within $1'$ from the XIS aim point. This implies that the efficiency of all the XRT-Is is more than 97 % even at 10 keV when we observe a point source on the XIS aimpoint.

By assuming the detector efficiency is constant over the field of view, we determined the vignetting function as shown in Figure 5.7. The vignetting function is narrower in higher energy. The averaged effective area over the detector size of XIS ($17.8'$x$17.8'$) is 60%, 60% and 50% of the E.A on axis at 1.5, 4.5 and 8.0 keV, respectively.

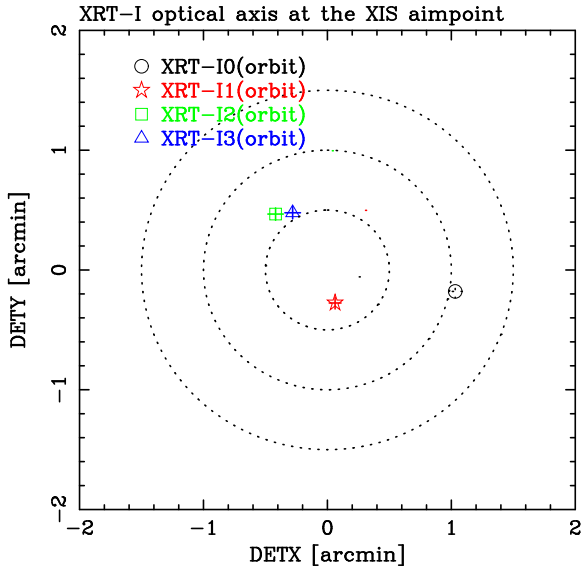

Figure 5.6: Optical axis directions of the XIS-S0 through S3. The optical axis of the XRT-I0 (XIS-S0), for example, locates at ($1.'0$, $-0.'2$), which implies that the maximum throughput is achieved for XRT-I0 when the satellite points at the XIS aimpoint.

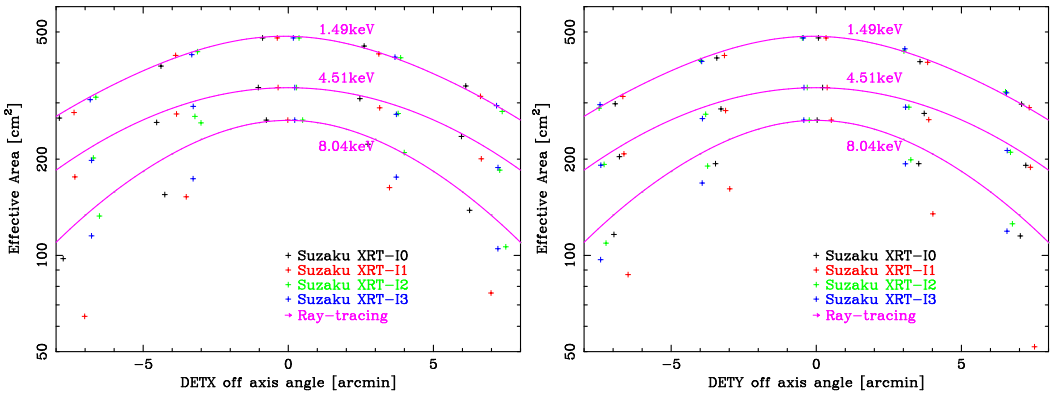

Figure 5.7: Vignetting curves of XRT-I at three different energies of 1.5, 4.5 and 8.0 keV. The three solid lines in the plots correspond to a parameter of ray-tracing program while the crosses are the preliminary XRT-I effective area "inferred" from the Crab pointings with some assumptions. The XRT-I effective area shown here does not includes either the quantum efficiency of the detector or transmissivity of the thermal shield and the optical blocking filter.

5.2.3 Stray Light

In-flight stray-light observations were carried out with Crab at off-axis angles of 20′ (4 pointings), 50′ (4 pointing) and 120′ (4 pointing) in August and September. We show an example of 20′-off image of XRT-I3 together with simulation results of the same off-axis angle for the cases with and without the pre-collimator in Fig. 5.8. It is seen that the pre-collimator works for reducing the stray light in orbit.

Figure 5.9 shows angular responses of the XRT-I at 1.5 and 4.5 keV up to 2 degrees. The effective area is normalized at on-axis. The integration area is corresponding to the detector size of XIS ($17'.8 \times 17'.8$). The plots are necessary to plan observations of diffuse sources or faint emissions near bright sources, such as outskirts of cluster of galaxies, diffuse objects in the Galactic plane, SN 1987A, etc.

The three solid lines in the plots correspond to different parameters of ray-tracing program while the crosses are the normalized effective area using the Crab pointings. For example, the effective area of the stray lights at 1.5 keV is $\sim 10^{-3}$ at angles smaller than 70 arcmin off axis and $< 10^{-3}$ at angles larger than 70 arcmin off. The measured flux of stray lights are in good agreement with that of raytracing within an order. This ray-tracing routine will be incorporated in the ARF generator before the AO1 deadline.

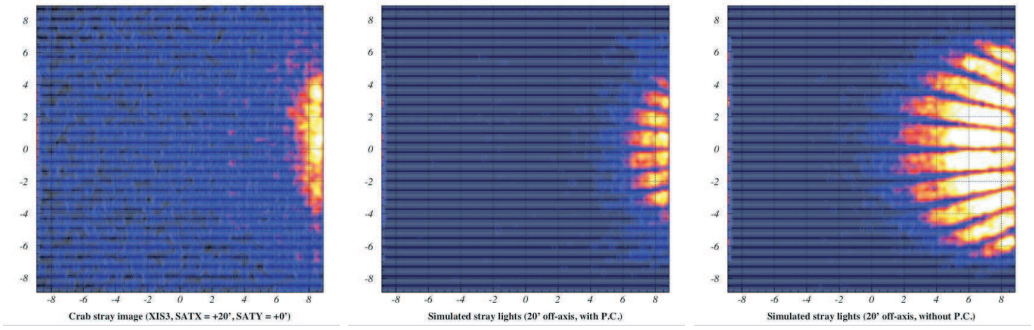

Figure 5.8: *left*: A $-20'$-off image of the Crab nebula taken with XIS3. *middle*: A simulated image of a point source at $-20'$ off with the pre-collimator. *right*: The same as the middle panel but without the pre-collimator. The pre-collimator properly works in orbit.

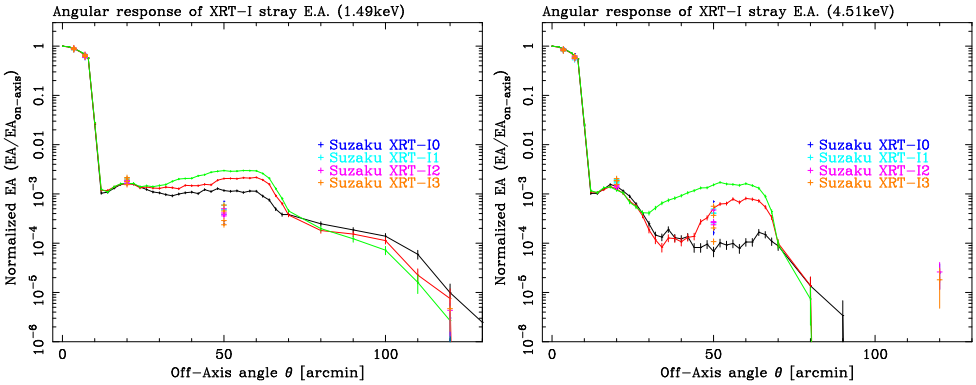

Figure 5.9: Angular responses of the XRT-I at 1.5 (left) and 4.5 keV (right) up to 2 degrees. The effective area is normalized at on-axis. The integration area is corresponding to the detector size of XIS ($17'.8 \times 17'.8$). The three solid lines in the plots correspond to different parameters of ray-tracing program while the crosses are the normalized effective area using the Crab pointings.

Chapter 6

X–ray Imaging Spectrometer (XIS)

6.1 Overview of the XIS

Figure 6.1: The four XIS detectors before installation onto *Suzaku*.

Suzaku has four X–ray Imaging Spectrometers (XISs), which are shown in Figure 6.1. These employ X–ray sensitive silicon charge-coupled devices (CCDs), which are operated in a photon-counting mode, similar to that used in the ASCA SIS, *Chandra* ACIS, and *XMM-Newton* EPIC. In general, X-ray CCDs operate by converting an incident X–ray photon into a charge cloud, with the magnitude of charge proportional to the energy of the absorbed X–ray. This charge is then shifted out onto the gate of an output transistor via an application of time-varying electrical potential. This results in a voltage level (often referred to as "pulse height") proportional to the energy of the X–ray photon.

The four *Suzaku* XISs are named XIS-S0, S1, S2 and S3, each located in the focal plane of

an X–ray Telescope; those telescopes are known respectively as XRT-I0, XRT-I1, XRT-I2, and XRT-I3. Each CCD camera has a single CCD chip with an array of 1024 × 1024 picture elements ("pixels"), and covers an $18' \times 18'$ region on the sky. Each pixel is 24 μm square, and the size of the CCD is 25 mm × 25 mm. One of the XISs, XIS-S1, uses a back-side illuminated CCDs, while the other three use front-side illuminated CCDs. The XIS has been partially developed at MIT (CCD sensors, analog electronics, thermo-electric coolers, and temperature control electronics), while the digital electronics and a part of the sensor housing were developed in Japan, jointly by Kyoto University, Osaka University, Rikkyo University, Ehime University, and ISAS.

A CCD has a gate structure on one surface to transfer the charge packets to the readout gate. The surface of the chip with the gate structure is called the "front side". A front-side illuminated CCD (FI CCD) detects X-ray photons that pass through its gate structures, i.e. from the front side. Because of the additional photo-electric absorption at the gate structure, the low-energy quantum detection efficiency (QDE) of the FI CCD is rather limited. Conversely, a back-side illuminated CCD (BI CCD) receives photons from "back," or the side without the gate structures. For this purpose, the undepleted layer of the CCD is completely removed in the BI CCD, and a thin layer to enhance the electron collection efficiency is added in the back surface. A BI CCD retains a high QDE even in sub-keV energy band because of the absence of gate structure on the photon-detection side. However, a BI CCD tends to have a slightly thinner depletion layer, and the QDE is therefore slightly lower in the high energy band. The decision to use only one BI CCD and three FI CCDs was made because of both the slight additional risk involved in the new technology BI CCDs and the need to balance the overall efficiency for both low and high energy photons.

To minimize the thermal noise, the sensors need to be kept at $\sim -90°$C during observations. This is accomplished by thermo-electric coolers (TECs), controlled by TEC Control Electronics, or TCE. The Analog Electronics (AE) drives the CCD clocks, reads and amplifies the data from the CCDs, performs the analog-to-digital conversion, and routes the signals to the Digital Electronics (DE). The AE and TCE are located in the same housing, and together, they are called the AE/TCE. *Suzaku* has two AE/TCEs; AE/TCE01 is used for XIS-S0 and S1, and AE/TCE23 is used for XIS-S2 and S3. The digital electronics system for the XISs consists of two Pixel Processing Units (PPU) and one Main Processing Unit (MPU); PPU01 is associated with AE/TCE01, and PPU23 is associated with AE/TCE23. The PPUs receive the raw data from AE, carry out event detection, and send event data to the MPU. The MPU edits and packets the event data, and sends them to the satellite's main digital processor.

To reduce contamination of the X–ray signal by optical and UV light, each XIS has an Optical Blocking Filter (OBF) located in front of it. The OBF is made of polyimide with a thickness of 1000 Å, coated with a total of 1200 Å of aluminum (400 Å on one side and 800 Å on the other side). To facilitate the in-flight calibration of the XISs, each CCD sensor has two ^{55}Fe calibration sources. One is installed on the door to illuminate the whole chip, while the other is located on the side wall of the housing and is collimated in order to illuminate two corners of the CCD. The door-mounted source will be used for initial calibration only; once the door is opened, it will not illuminate the CCD. The collimated source can easily be seen in two corners of each CCD. A small number of these X–rays scatter onto the entire CCD. In addition to the emission lines created by these sources, we can utilize a new feature of the XIS CCDs, "charge injection capability," to assist with calibration. This allows an arbitrary amount of charge to be input to the pixels at the top row of the imaging region (exposure area), i.e. the far side from the frame-store region. The charge injection capability may be used to measure the CTI (charge transfer inefficiency) of each column, or even to reduce the CTI. How the charge injection capability will be used is still in progress as of this writing.

Fig. 6.2 provides a schematic view of the XIS system. Charge clouds produced in the CCD by the X–rays focused by the XRT are accumulated on the exposure area for a certain exposure period

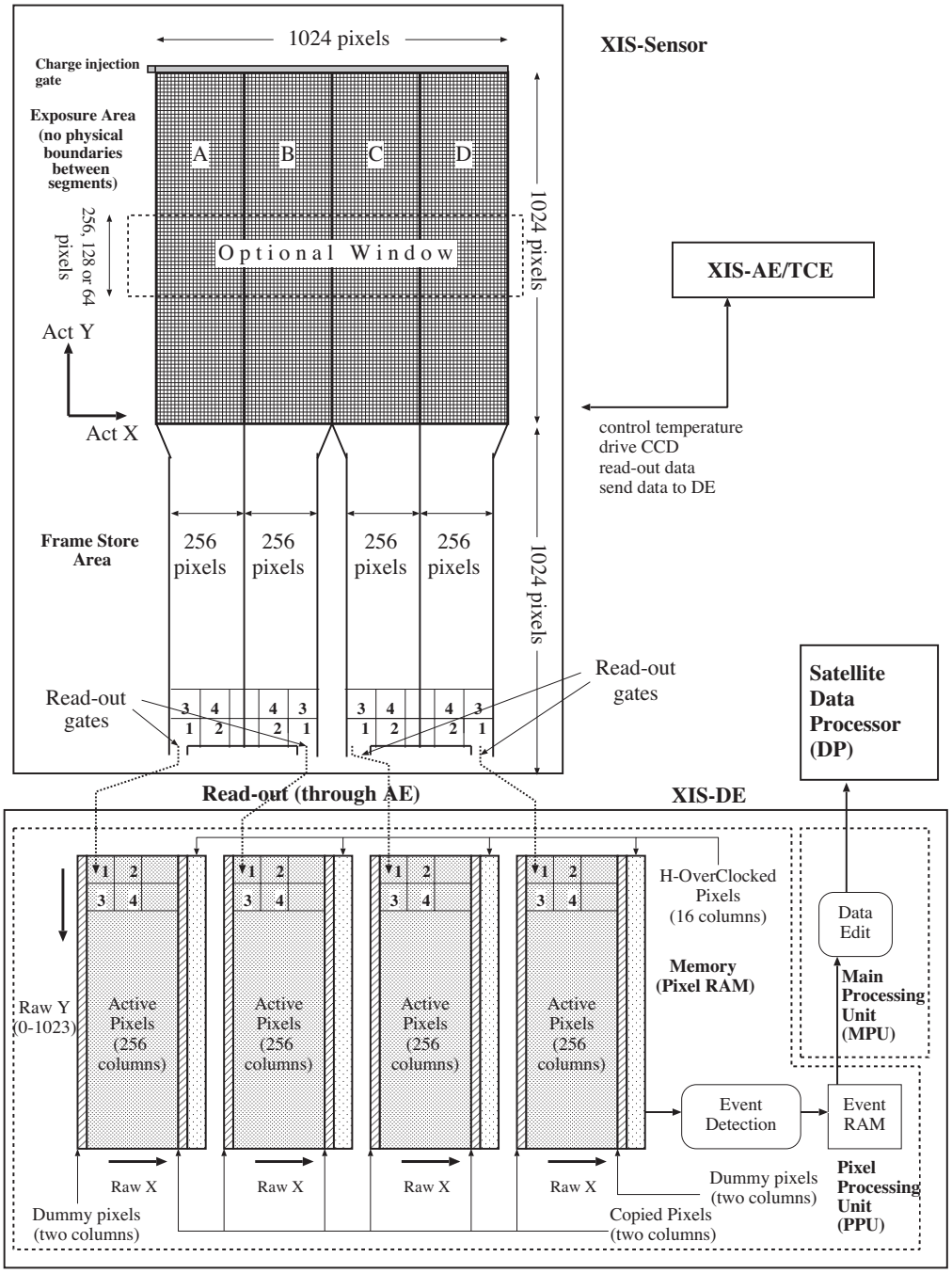

Figure 6.2: One XIS instrument. Each XIS consists of a single CCD chip with 1024 × 1024 X–ray sensitive cells, each 24 μm square. *Suzaku* contains four CCD sensors (XIS-S0 to S3), two AE/TCUs (AE/TCE01 and AE/TCE23), two PPUs (PPU01 and PPU23), and one MPU. AE/TCU01 and PPU01 service XIS-S0 and XIS-S1, while AE/TCE23 and PPU23 service XIS-S2 and XIS-S3. Three of the XIS CCDs are front-illuminated (FI) and one (XIS-S1) is back-illuminated (BI).

(typically 8 s in the "normal" mode), and the data are transferred to the Frame Store Area (FSA) after each exposure. Data stored in the Frame Store Area are read-out sequentially by the AE, and sent to the PPU after the conversion to the digital data. The data are put into the memory in PPU named Pixel RAM. Subsequent data processing is done by accessing the Pixel RAM.

6.2 CCD Pixels and Coordinates

A single XIS CCD chip consists of four segments (marked A, B, C and D in Fig. 6.2) and correspondingly has four separate readout nodes. Pixel data collected in each segment are read out from the corresponding readout node and sent to the Pixel RAM. In the Pixel RAM, pixels are given RAWX and RAWY coordinates for each segment in the order of the readout, such that RAWX values are from 0 to 255 and RAWY values are from 0 to 1023. These physical pixels are named *Active pixels*.

In the same segment, pixels closer to the read-out node are read-out faster and stored in the Pixel RAM faster. Hence, the order of the pixel read-out is the same for segments A and C, and for segments B and D, but different between these two segment pairs, because of the different locations of the readout nodes. In Fig. 6.2, numbers 1, 2, 3 and 4 marked on each segment and Pixel RAM indicate the order of the pixel read-out and the storage in the Pixel RAM.

In addition to the Active pixels, the Pixel RAM stores the *Copied pixels*, *Dummy pixels* and *H-Over-Clocked pixels* (cf. Fig. 6.2). At the borders between two segments, two columns of pixels are copied from each segment to the other. Thus these are named Copied pixels. On both sides of the outer segments, two columns of empty Dummy Pixels are attached. In addition, 16 columns of H-Over-Clocked pixels are attached to each segment.

Actual pixel locations on the chip are calculated from the RAW XY coordinates and the segment ID during ground processing. The coordinates describing the actual pixel location on the chip are named ACT X and ACT Y coordinates (cf. Fig. 6.2). It is important to note that the RAW XY to ACT XY conversion depends on the on-board data processing mode (cf. § 6.4).

6.3 Pulse Height Determination, Residual Dark-current Distribution, and Hot Pixels

When a CCD pixel absorbs an X–ray photon, the X–ray is converted to an electric charge, which in turn produces a voltage at the analog output of the CCD. This voltage ("pulse-height") is proportional to the energy of the incident X–ray. In order to determine the true pulse-height corresponding to the input X–ray energy, it is necessary to subtract the *Dark Levels* and correct possible *optical Light Leaks*.

Dark Levels are non-zero pixel pulse-heights caused by leakage currents in the CCD. In addition, optical and UV light may enter the sensor due to imperfect shielding ("light leak"), producing pulse heights that are not related to X–rays. In the case of the ASCA SIS, these were handled via a single mechanism: Dark Levels of 16×16 pixels were sampled and their (truncated) average was calculated for every exposure. Then the same average Dark Level was used to determine the pulse-height of each pixel in the sample. After the launch of ASCA, it was found that the Dark Levels of different pixels were actually different, and their distribution around the average did not necessarily follow a Gaussian. The non-Gaussian distribution evolved with time (referred to as Residual Dark-current Distribution or RDD), and resulted in a degradation of the energy resolution due to incorrect Dark Levels.

For the *Suzaku* XIS, Dark Levels and Light Leaks are calculated separately in normal mode. Dark Levels are defined for each pixel; those are expected to be constant for a given observation. The PPU calculates the Dark Levels in the Dark Initial mode (one of the special diagnostic modes of the XIS); those are stored in the Dark Level RAM. The average Dark Level is determined for each pixel, and if the dark level is higher than the hot-pixel threshold, this pixel is labeled as a *hot pixel*. Dark Levels can be updated by the Dark Update mode, and sent to the telemetry by the Dark

Frame mode. Unlike the case of ASCA, Dark Levels are not determined for every exposure, but the same Dark Levels are used for many exposures unless they are initialized or updated. Analysis of the ASCA data showed that Dark Levels tend to change mostly during the SAA passage of the satellite. Dark Update mode may be employed several times a day after the SAA passage.

Hot pixels are pixels which always output over threshold pulse-heights even without input signals. Hot pixels are not usable for observation, and their output has to be disregarded during scientific analysis. The ASCA SIS did not identify hot pixels on-board, and all the hot pixel data were telemetered and removed during the data analysis procedure. The number of hot pixels increased with time, and eventually occupied significant parts of the telemetry. In the case of XIS, hot pixels are detected on-board by the Dark Initial/Update mode, and their positions and pulse-heights are stored in the Hot-pixel RAM and sent to the telemetry. Thus, hot pixels can be recognized on-board, and they are excluded from the event detection processes. It is also possible to specify the hot pixels manually. There are, however, some pixels which output over threshold pulse-heights intermittently. Such pixels are called flickering pixels. It is difficult to identify and remove the flickering pixels on board; they are inevitably output to the telemetry and need to be removed during the ground processing. Flickering pixels sometimes cluster around specific columns, which makes it relatively easy to identify.

The Light Leaks are calculated on board with the pulse height data after the subtraction of the Dark Levels. A truncated average is calculated for 64×64 pixels (this size may be changed in the future) in every exposure and its running average produces the Light Leak. Thus, the Light Leak is basically the same as the Dark Level in ASCA SIS.

The Dark Levels and the Light Leaks are merged in the parallel-sum (P-Sum) mode, so Dark Update mode is not available in P-Sum mode. The Dark Levels, which are defined for each pixel as the case of the normal mode, are updated every exposure. It may be considered that the Light Leak is defined for each pixel in P-Sum mode.

6.4 On-board Event Analysis

The main purpose of the on-board processing of the CCD data is to reduce the total amount transmitted to ground. For this purpose, the PPU searches for a characteristic pattern of charge distribution (called an event) in the pre-processed (post- Dark Levels and Light Leaks subtraction) frame data. When an X–ray photon is absorbed in a pixel, the photoionized electrons can spread into at most four adjacent pixels. An event is recognized when a valid pulse-height (one between the Event Lower and Upper Thresholds) is found that exceeds the pulse-heights in the eight adjacent pixels (e.g. it is the peak value in the 3×3 pixel grid). In P-Sum mode, only the horizontally adjacent pixels are considered. The Copied and Dummy pixels ensure that the event search is enabled on the pixels at the edges of each segment. Again, in the case of P-Sum mode only the inner one of the two columns of Copied or Dummy pixels on each side of the Segment is necessary and used. The RAW XY coordinates of the central pixel are considered the location of the event. Pulse-height data for the adjacent 5×5 square pixels (or in P-Sum mode 3 horizontal pixels) are sent to the Event RAM as well as the pixel location.

The MPU reads the Event RAM and edits the data to the telemetry format. The amount of information sent to telemetry depends on the editing mode of the XIS. All the editing modes (in normal mode; see §6.5) are designed to send the pulse heights of at least 4 central pixels of an event to the telemetry, because the charge cloud produced by an X-ray photon can spread into at most 4 pixels. Information of the surrounding pixels may or may not output to the telemetry depending on the editing mode. The 5×5 mode outputs the most detailed information to the telemetry, i.e. all 25 pulse-heights from the 5×5 pixels containing the event. The size of the telemetry data per

Option	Effective area (nominal: 1024 × 1024 pixels)	Exposure time (in 8 s period)
None	1024 × 1024 pixels	8 s
Burst	1024 × 1024 pixels	$(n/256) \times 8$ s × 1 exposure
Window	256 × 1024 pixels	2 s × 4 exposures
	128 × 1024 pixels	1 s × 8 exposures
Burst & Window	256 × 1024 pixels	$(n/64) \times 2$ s × 4 exposure
	128 × 1024 pixels	$(n/32) \times 1$ s × 8 exposure

Note: n is an integer.

Table 6.1: Effective area and exposure time for different burst and window options

event is reduced by a factor of 2 in 3 × 3 mode, and another factor of 2 in 2 × 2 mode. Details of the pulse height information sent to the telemetry are described in the next section.

6.5 Data Processing Modes

There are two different kinds of on-board data processing modes. The *Clock modes* describe how the CCD clocks are driven, and determine the exposure time, exposure region, and time resolution. The Clock modes are determined by a kind of program loaded to the AE. The *Editing modes* specify how detected events are edited, and determine the formats of the XIS data telemetry. Editing modes are determined by the digital electronics.

It is possible to select different mode combinations for the four XISs independently. However, we expect that most observations will use all four in Normal 5 × 5 or 3 × 3 Mode (without Burst or Window options). Other modes are useful for bright sources (when pile-up or telemetry limitations are a concern) or if a higher time resolution (<8 s) is required.

6.5.1 Clock Modes

The following two kinds of Clock Modes are available. Furthermore, two options (Window and Burst options) may be used in combination with the Normal Mode.

- **Normal Mode:** If neither *Window* nor *Burst* option (see below) is specified, the exposure time is 8 seconds, and all the pixels on the CCD are read out every 8 seconds. This can be combined with either of the 5 × 5, 3 × 3, and 2 × 2 Editing modes.
- **Parallel Sum Mode:** The pixel data from multiple rows are summed in the Y-direction on the CCD, and the sum is put in the Pixel RAM as a single row. The number of rows to add is commandable. Parallel Sum mode can be used only with the Timing Editing mode, and the Y coordinate is used to determine the event arrival time. As a result, no spatial resolution is available in the Y-direction. The time resolution of the Parallel Sum Mode is 8 s/1024 ∼ 7.8 ms.

6.5.2 Window and Burst Options

Table 6.1 indicates how the effective area and exposure time are modified by the Burst and Window options.

In the Normal Clock mode, the *Window* and *Burst* options can modify the effective area and exposure time, respectively. The two options are independent, and may be used simultaneously. These options cannot be used with the Parallel Sum Clock mode.

- **Burst Option:** All the pixels are read out every 8 seconds (if the Window option is not specified), but the exposure time can be chosen arbitrarily (with a 1/32 second step) within the read-out interval. This option may be used to avoid event pile-up when observing a bright source. However, a dead time is introduced in the exposure. If the exposure is t s, there is a $8 - t$ s dead-time every 8 s.
- **Window Option:** This option allows shorter exposure times by reading out more frequently only a portion of the CCD. Only the parts of the chip within the Y-direction range specified by the commandable Window is used for exposure (cf. Fig. 6.2). The Window width in the Y-direction is either 256, 128 pixels around the aimpoint. When the Window width is 256 pixels, the exposure time becomes a quarter of that without the Window option (i.e. 2 s), and the Pixel RAM is filled with the data from four successive exposures. Similarly, when the Window width is 128 pixels, the exposure time becomes 1/8 of that without the Window option respectively, and the Pixel RAM is filled with the data from 8 successive exposures.

We show in Fig. 6.3 the time sequence of exposure, frame-store transfer, CCD readout, and storage to the pixel RAM (in PPU) in normal mode with or without Burst/Window option. Note that a dead time is introduced when the Burst option is used.

6.5.3 Editing Modes

We explain only the observation modes here. Three modes (5×5, 3×3, and 2×2) are usable in normal modes, and only the timing mode in the P-Sum mode.

Observation Modes

- 5×5 **mode:** All the pulse heights of the 25 pixels centered at the event center are sent to the telemetry. This is used with the Normal Clock mode.
- 3×3 **mode:** Pulse heights of the 9 pixels centered at the event center are sent to the telemetry with the 1-bit information (pulse height larger than the Split Threshold Outer or not) for the surrounding 16 pixels. This is used with the Normal Clock mode.
- 2×2 **mode:** Pulse heights of the 2×2 square pixels are sent to the telemetry. The 2×2 pixels are selected to include the event center, second highest pixel in the cross centered at the event center, and the 3rd (or 4th) highest pixel in the cross. The 1-bit information (pulse height larger than the Split Threshold Outer or not) of the 8-attached pixels is also output to the telemetry. This is used with the Normal Clock mode.
- **Timing mode:** Total pulse height and the *Grades* of the event are output to the telemetry. Pulse heights of at most three pixels in the X-direction are summed to give the total pulse height if they are over the Inner Split Threshold. Position and number of pixels exceeding the threshold determines the *Grades*. This is used only with the P-Sum Clock mode. Window and Burst Options are not available in the Timing mode.

We show in Fig. 6.4 the pixel pattern whose pulse height or 1-bit information is sent to the telemetry. We do not assign grades to an event on board in the Normal Clock mode. This means

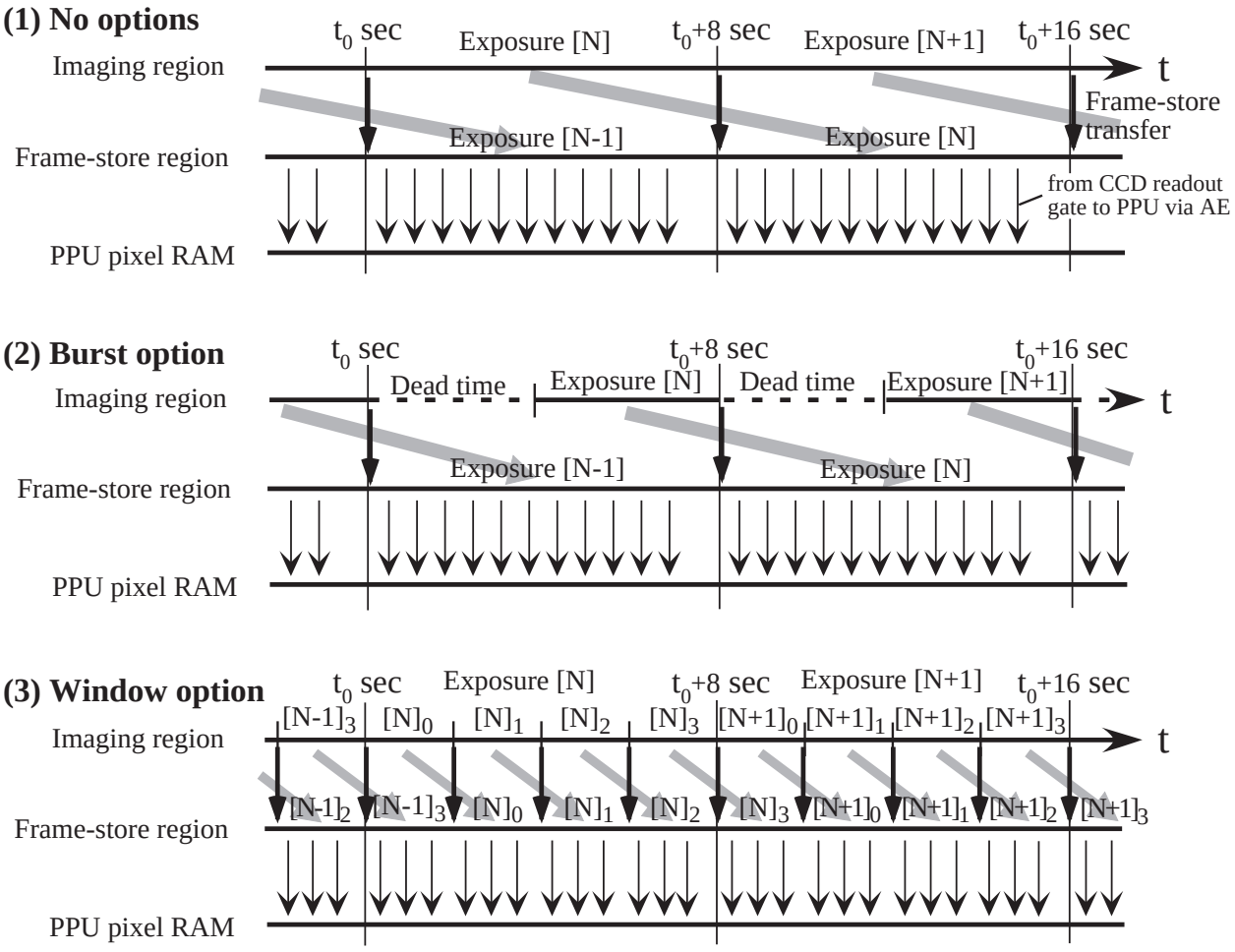

Figure 6.3: Time sequence of the exposure, frame-store transfer, CCD readout, and data transfer to the pixel RAM in PPU is shown (1) in normal mode without options, (2) in normal mode with Burst option, and (3) in normal mode with Window option. In this example, the 1/4 Window option is assumed.

that a dark frame error, if present, can be corrected accurately during the ground processing even in 2 × 2 mode. The definition of the grades in P-Sum mode is shown in Fig. 6.5.

There are slight differences between the 5×5, 3×3 and 2×2 modes. We currently neglect these differences between the 5×5 and 3×3 modes but not with the 2×2 mode as this mode is slightly different from 3×3 or 5×5 mode. This difference is smaller in the FI CCDs and is larger in BI CCD. For example, although the CTE effect on gain (see §6.8) can be corrected in both 2×2 and 3×3 modes, the accuracy of the gain correction is slightly worse in 2×2 mode. CTE also affect the quantum detection efficiency, and therefore the correction of the CTE effect on QDE is also worse in 2×2 mode. Although the *Suzaku* XIS team may eventually need to prepare different calibration data for the 2×2 mode, the differences are not very large in the FI CCD. Therefore at present, you may be able to use the calibration data of 3×3 (5×5) mode for 2×2 FI data, unless you require high accuracy. However, the BI chip has a relatively large CTI and the difference between the 2×2 and 3×3 modes is also large (compared to the FI chips). For this reason, we discourage using the 2×2 mode with the BI chip, although it is usable for the FI CCDs, and has been used with bright sources already. We note that the XIS team cannot guarantee accurate calibration of the 2x2 mode for the BI chip. Suzaku operation team will try not to use the 2×2 mode for the BI chip unless

otherwise specified.

Besides the observation modes given above, the XIS instrument has several diagnostic modes, used primarily in determining the dark current levels. It is unlikely that those would be used by guest observers.

Note on the timing mode

In timing mode, data quality may be significantly degraded compared to the normal mode. Degradation is possible in terms of the background rate, the energy resolution, the effective area, the energy range, among others. Users should be aware of this when choosing the timing mode.

Because only one dimensional information is available in timing mode, distinction between X-ray and non-X-ray events becomes inaccurate. This means that timing mode has significantly higher non-X-ray background than the normal mode. Actual background rate in timing mode is under investigation using the flight data. We therefore discourage the use of the timing mode for a faint source.

As described in 6.3 the Dark Levels are defined in each pixel in timing mode. From the analysis of the flight data, it is apparent that the fluctuation of the Dark Levels due to the particle events is rather large in timing mode. The fluctuation may introduce an excess noise in the calculation of the pulse height. This means that the energy resolution in the timing mode may be slightly worse compared to the normal mode. Furthermore, very low energy part of the data (say $<$0.4 keV) might not be available in the timing mode. A more complete determination of the usable energy range in the timing mode is under investigation now.

Effective area of the CCDs may change in the timing mode. There are some numbers of hot pixels in the CCDs. The hot pixels introduce only a very small dead area in normal mode. However, a hot pixel might kill a column in timing mode. This means that hot pixels could bring relatively large reduction in the effective area of CCDs. Furthermore, the reduction of effective area may not be stable because some hot pixels appear and disappear in time and the satellite attitude may fluctuate. Thus we do not recommend timing mode to measure the source flux accurately.

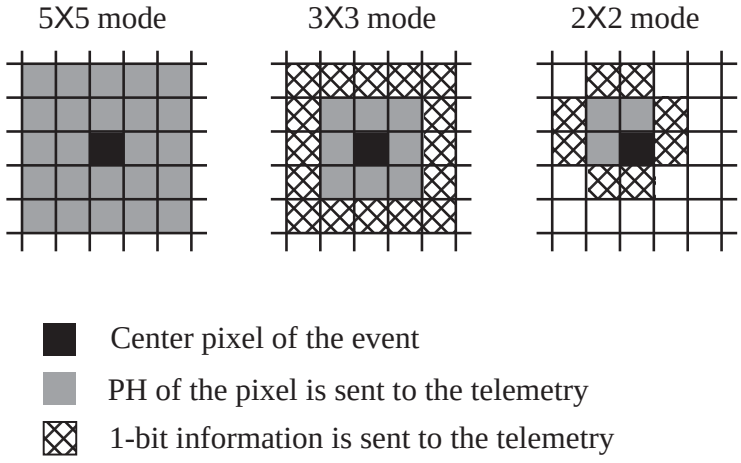

Figure 6.4: Information sent to the telemetry is shown for 5×5, 3×3, and 2×2 modes. 1-bit information means whether or not the PH of the pixel exceeds the outer split threshold. In 2×2 mode, the central 4 pixels are selected to include the second and the third (or fourth) highest pixels among the 5 pixels in a cross centered at the event center.

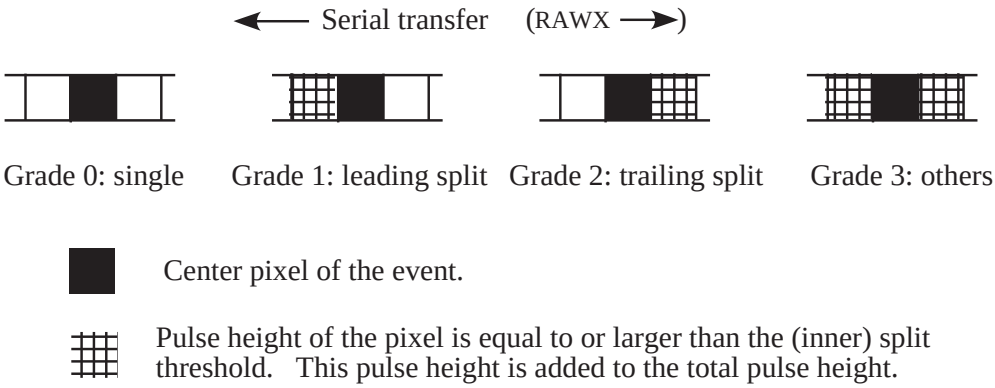

Figure 6.5: Definition of the grades in the P-Sum/timing mode. Total pulse height and the grade of the event are output to the telemetry. Note that the grades are defined referring to the direction of the serial transfer, so the central pixel of a grade 1 event has the *larger* RAWX value, while the opposite is true for a grade 2 event.

6.5.4 Discriminators

Two kinds of discriminators, area and grade discriminators, can be applied during the on-board processing. The grade discriminator is available only in the timing mode.

The area discriminator is used when we want to reject some (or most) of the frame data from the event extraction. The discriminator works on the Pixel RAM. When the discriminator is set, a part of the Pixel RAM is not used for the event extraction. This may be useful when a bright source is present in the XIS field of view other than the target source. If we set the discrimination area to include only the bright source, we can avoid outputting unnecessary events to the telemetry. Only a single, rectangular area can be specified in a segment for discrimination. Either inside or outside of the area can be rejected from the event extraction. The area discriminator works on the Pixel RAM, not for the physical area of the CCD. This is important when we apply the discriminator with the window option.

The Grade discriminator is used only in the timing mode. Any combination of the 4 grades can be selected to discriminate the grade for telemetry output.

Suzaku does not have the level discriminator which was used in ASCA SIS. The same function can be realized, however, by changing the event threshold.

As of this writing, the XIS team plans to add one more discriminator, a class discriminator, to XIS DE. The class discriminator will become available before the start of AO1. The class discriminator classify the events into two classes, “X-rays” and “others,” and output only the ”X-ray” class to the telemetry when it is enabled. The “other” class is close to, but slightly different from grade 7. When XIS points to blank sky, more than 90% of the detected events is particle events (mostly grade 7). If we reject these particle events on board, we can make a substantial saving in telemetry usage. This is especially useful when the data rate is medium or low. The class discriminator realizes such a function in a simple manner. When all the 8 pixels surrounding the event center exceeds the Inner Split Threshold, the event is classified as the “other” class, and the rest of the events as the “X-ray” class. With such a simple method, we can reject more than three quarter of the particle events. The class discriminator works only for 5x5 and 3x3 modes. It is not available in 2x2 and timing mode.

6.6 Photon pile-up

The XIS is essentially a position-sensitive integrating instrument, with the nominal interval between readouts of 8 s. If during the integration time one or more photons strike the same CCD pixel, or one of its immediate neighbors, these cannot be correctly detected as independent photons: this is the phenomenon of photon pile-up. Here, the modest angular resolution of the *Suzaku* XRT is an advantage: the central 3×3 pixel area receives 2% of the total counts of a point source, and ∼10% of the counts fall within ∼0.15 arcmin of the image center. We calculated the count rate at which 50% of the events within the central 3×3 pixels are piled-up (the pile-up fraction goes down as we move out of the image center; this fraction is <5% for the 0.15 arcmin radius) — although we offer no formal justification for this particular limit, this is compatible with our ASCA SIS experience (i.e., at this level, the pile-up effects do not dominate the systematic uncertainties). **In practice, point sources with < 100 cts/exposure can be observed in the normal mode (full window)**. For somewhat brighter sources, window options can be used to reduce the exposure time per frame (the count rate limit is inversely proportional to the exposure time — 1/8 window option reduces the exposure time from 8 s to 1 s, and raises the limit from ~ 12.5 cts/s to ∼100 cts/s). For even brighter sources, timing mode may be used: because of the extremely short effective exposure time (8 s/1024 $\sim$ 7.8 ms), the pile-up limit is several thousand cps (despite the on-board summing of rows and the one dimensional nature of the event detection algorithm).

In case of questions, *Suzaku* personnel at ISAS/JAXA or the NASA *Suzaku* GOF will work with the observers to assure the optimum yield of every observation via selection of the best XIS mode for a given target.

6.7 XIS background rate and the telemetry limit

All four XISs have low backgrounds, due to a combination of the *Suzaku* orbit and the instrumental design. Below 1 keV, the high sensitivity and energy resolution of the XIS-S1 combined with this low background means that *Suzaku* is the superior instrument for observing soft sources with low surface brightness. At the same time, the large effective area at Fe K (comparable to the XMM pn) combined with this low background make *Suzaku* a powerful tool for investigating hot and/or high energy sources as well.

In the XIS, the background originates from the cosmic X–ray background (CXB) combined with charged particles (the non-X–ray background, or NXB). Currently, flickering pixels are a negligible component of the backgrond. When observing the dark earth (*i.e.* the NXB), the background rate between 1-12 keV in is 0.11 cts/s in the FI CCDs and 0.40 cts/s in the BI CCD; see Figure 6.6. Note that these are the fluxes after the grade selection is applied with only grade 0, 2, 3, 4 and 6 selected. There are also fluorescence features arising from the calibration source as well as material in the XIS and XRTs. The Mn lines are due to the scattered X-rays from the calibration sources. As shown in Table 6.2 the Mn lines are almost negligible except for XIS-S0. The O lines are mostly contamination from the day earth (6.7.2). The other lines are fluorescent lines from the material used for the sensor. Table 6.2 shows the current best estimates for the strength of these emission features, along with their 90% upper and lower limits.

The background rate on the FI chips (including all the grades) is normally less than 400 counts/frame (50 cts/s) when no class discriminator is applied. On the BI chip, the rate is normally less than 150 counts/frame (18.75 cts/s). The background rate on the FI chips is expected to reduce significantly when the class discriminator is applied. But little change is anticipated for the BI chip. Since 5×5, 3×3, and 2×2 modes require on average 40, 20, and 10 bytes per event, the

Table 6.2: Major XIS Background Emission Lines

Line	Energy keV	XIS-S0 10^{-9} ct/s/pix	XIS-S1 10^{-9} ct/s/pix	XIS-S2 10^{-9} ct/s/pix	XIS-S3 10^{-9} ct/s/pix
O K	0.5249	18.5 ± 0.5	$69.3^{+2.7}_{-2.6}$	$14.3^{+1.5}_{-1.3}$	$14.1^{+1.1}_{-1.2}$
Al K	1.49	1.98 ± 0.23	3.01 ± 0.51	$1.50^{+0.31}_{-0.28}$	$1.57^{+0.25}_{-0.23}$
Si K	1.740	$0.299^{+0.2080}_{-0.2074}$	2.21 ± 0.45	$0.0644(< 0.282)$	$0.543^{+0.212}_{-0.213}$
Au M	2.1229	0.581 ± 0.234	$1.13^{+0.280}_{-0.291}$	$0.359^{+0.211}_{-0.212}$	$6.69^{+2.91}_{-2.90}$
Mn Kα	5.898	$8.35^{+0.36}_{-0.34}$	0.648 ± 0.289	$0.299^{+0.209}_{-0.2086}$	$0.394^{+0.181}_{-0.18}$
Mn Kβ	6.490	$1.03^{+0.22}_{-0.216}$	$0.294(< 0.649)$	$0.00(< 0.111)$	$0.428^{+0.225}_{-0.226}$
Ni Kα	7.470	7.20 ± 0.31	6.24 ± 0.53	$3.78^{+0.26}_{-0.25}$	$7.13^{+0.36}_{-0.37}$
Ni Kβ	8.265	0.583 ± 0.183	$1.15^{+0.5}_{-0.489}$	0.622 ± 0.206	$0.983^{+0.247}_{-0.249}$
Au Lα	9.671	$3.52^{+0.27}_{-0.28}$	$3.28^{+1.16}_{-0.99}$	$1.88^{+0.31}_{-0.28}$	$3.54^{+0.36}_{-0.35}$
Au Lβ	11.514	$2.25^{+0.73}_{-0.59}$	2.91 ± 1.29	$0.752^{+0.428}_{-0.304}$	$2.67^{+0.61}_{-0.53}$

Note: Typical accumulation time are 110-160 ks

Table 6.3: Recommended XIS modes for different sources

Rate[1] cts/s	Telemetry Mode High	Medium	Clock
0–20	5×5	3×3	Normal
$\sim 20 - 100$	5×5	3×3	Window (avoid pileup)
$\sim 100 - 200$	3×3	FI: 2×2	Window (avoid pileup)
		BI: 3×3	
$\sim 200 - 1000$	FI: 2×2	FI: 2×2	Window (+ area discriminator)
	BI: 3×3	BI: 3×3	Burst (+ window)
> 1000	FI: 2×2	FI: 2×2	Burst (+ window)
	BI: 3×3	BI: 3×3	

Timing mode may be used depending on the objectives.
[1]Count rate for a single XIS sensor.

minimum telemetry required for any source is ~ 58 kbits/s for 5×5 mode, ~ 31 kbits/s for 3×3, and ~ 17 kbits/s for 2×2 mode, if no class discriminator is used. Due to staffing constraints, the available telemetry is slightly lower over the weekend. "High" rate telemetry is always 144 kbits/s, but "Medium" rate is 70 kbits/s during the week and 30 kbits/s over the weekend. Therefore, mission operation team tries not to allocate bright sources in the weekend. In sum, the recommended XIS mode for any combination of count rate and detector is given in Table 6.3.

Table 6.4: Telemetry limits (cnts/XIS/s)

Data rate	5×5	3×3	2×2	timing
Superhigh	260	520	1050	2370
High	120	250	500	1140
Medium (weekday)	60	120	240	550
Medium (weekend)	24	48	96	230
Low	15	30	60	150

Note: Nominal telemetry allocation for XIS and its equal distribution among the 4 sensors are assumed.

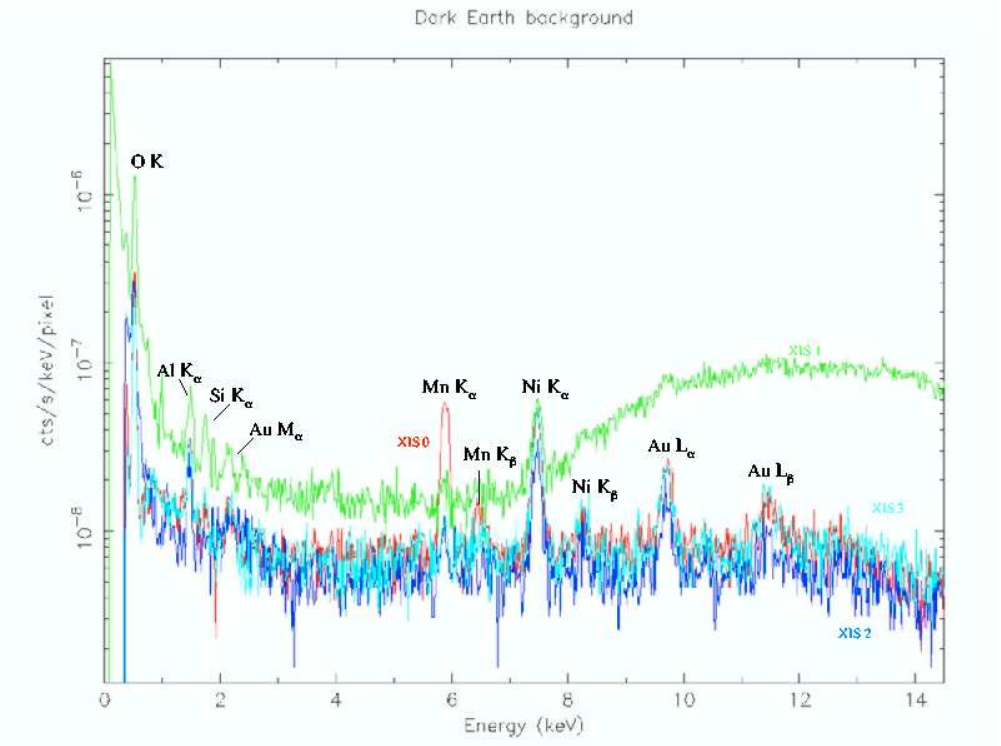

Figure 6.6: The XIS background rate for each of the four XIS detectors, with prominent fluorescent lines marked. These spectra are based on $\sim 110 - 160$ ksec of observations towards the dark Earth.

Table 6.4 shows the estimated telemetry limits of XIS in various editing modes and the telemetry data rates. As the NXB occupies some constant fraction of the telemetry, the rest is available for the X-ray events. The NXB rate of the FI CCD when the class discriminator is applied is not available as of the writing of this document; see the *Suzaku* websites for updated information (see App C). On the other hand, the NXB rate of the BI chip is normally less than ∼20 c/s regardless of the class discriminator. When we calculate the telemetry limits, we assumed a nominal telemetry allocation ratio among XIS, and HXD. The ratio depends on the data rate and may be changed in future. The telemetry limits also depend on the data compression efficiency. We apply a simple data compression algorithm to the event data, whose efficiency may depend on the energy spectrum of the source. Thus the telemetry limits listed in the table should be regarded as only approximate values.

6.7.1 Out-of-time events

X-ray photons detected during the frame-store transfer do not correspond to the true image, but instead appear as a streak or blur in the readout direction. These events are called out-of-time events., and they are an intrinsic feature of CCD detectors. Similar streaks are seen from bright sources observed with *Chandra* and *XMM-Newton*. Out-of-time events produce a tail in the image, which can be an obstacle to detecting a low surface brightness feature in an image around a bright source. Thus the out-of-time events reduce the dynamic range of the detector. Since XIS spends 25 ms in the frame-store transfer, about 0.3% ($= 0.025/8 \times 100$) of all events will be out-of-time events. However, because the orientation of the CCD chip is different among the sensors, one can in principle distinguish a true feature of low surface brightness and the artifact due to the out-of-time events by comparing the images from two or more XISs.

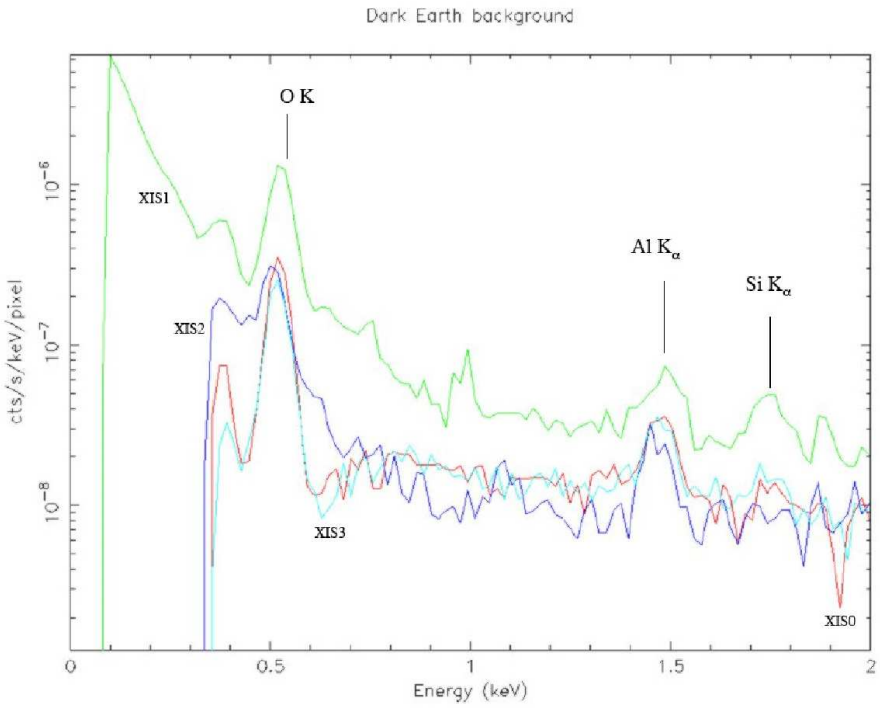

Figure 6.7: The XIS background rate for each of the four XIS detectors, showing only energies between 0.1-2.0 keV. Below 0.3 keV the background rate for the FI chips cannot be determined due to their low effective area.

6.7.2 Day Earth Contamination

When the XIS field of view is close to the day earth (i.e. Sun lit Earth), fluorescent lines from the atmosphere contaminate low-energy part of the XIS data, especially in the BI chip. Most prominent is the oxygen line, but the nitrogen line may be also noticed (see Fig. 6.7). These lines are mostly removed when we apply the standard data screening criteria (XIS FOV is at least 20 degree away from the day earth) during the ground processing. However, small amount of contamination can remain. This contamination may be further reduced if we subtract appropriate background. This subtraction, however, may be imperfect. Thus, when neutral oxygen or nitrogen lines are detected in the XIS data, contamination from day earth should be suspected.

6.8 Radiation Damage and On-board Calibration of the XIS

The performance of X-ray CCDs gradually degrades in the space environment due to the radiation damage. This generally causes an increase in the dark current and a decrease of the charge transfer efficiency (CTE). In the case of XIS, the increase of the dark current is expected to be small due to the low (–90°C) operating temperature of the CCD. However, a decrease in CTE is unavoidable. Thus, continuous calibration of CCD on orbit is essential to the good performance of the XIS. For this purpose, we use a radio isotope source and charge injection as explained below:

(i) Each XIS carries ^{55}Fe calibration sources near the two corners of the chip, which will be used to monitor the instrument gain.

(ii) Each XIS CCD is equipped with charge injection capability, which may be useful to measure

and even suppress CTI.

Nonetheless, it is difficult to predict based on existing data how well we can calibrate the long-term performance change of XIS on orbit.

Chapter 7

Hard X–ray Detector

Figure 7.1: The Hard X–ray Detector before installation.

The Hard X–ray Detector (HXD; see Figure 7.1) is a non-imaging, collimated hard X–ray scintillating instrument sensitive in the $\sim$ 10 keV to $\sim$ 600 keV band. It has been developed jointly by the University of Tokyo, Aoyama Gakuin University, Hiroshima University, ISAS/JAXA, Kanazawa University, Osaka University, Saitama University, SLAC, and RIKEN. Its main purpose is to extend the bandpass of the *Suzaku* observatory to the highest feasible energies, thus allowing broad-band studies of celestial objects.

The HXD sensor (HXD-S) is a compound-eye detector instrument, consisting of 16 main detectors (arranged as a 4×4 array) and the surrounding 20 crystal scintillators for active shielding. Each unit actually consists of two types of detectors: a GSO/BGO phoswich counter, and 2 mm-thick PIN silicon diodes located inside the well, but in front of the GSO scintillator. The PIN diodes are mainly sensitive below $\sim$ 60 keV, while the GSO/BGO phoswich counter (scintillator)

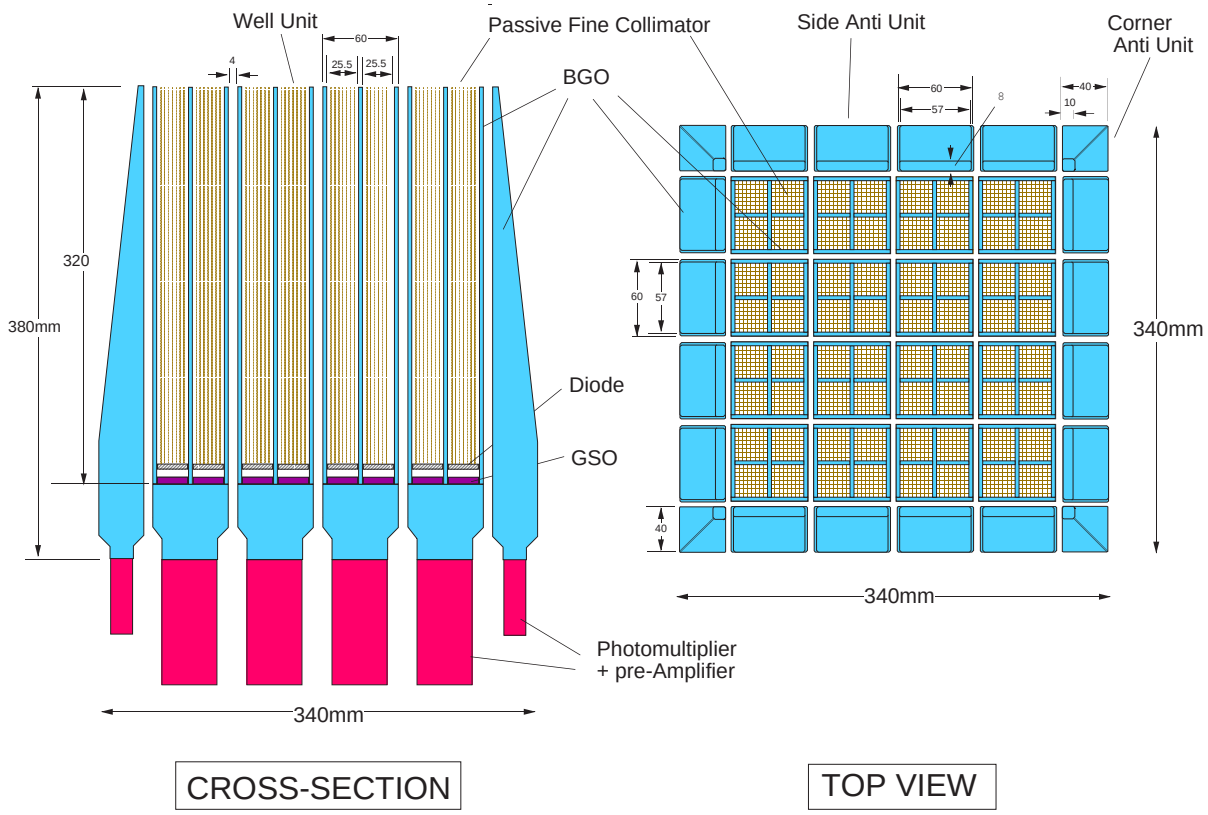

Figure 7.2: Schematic picture of the HXD instrument, which consists of two types of detectors: the PIN diodes located in the front of the GSO scintillator, and the scintillator itself.

is sensitive above $\sim$ 30 keV. The scintillator signals are read out by photomultiplier tubes. The schematic drawing of the HXD is given in Fig. 7.2. The HXD features an effective area of $\sim$ 160 cm^2 at 20 keV, and $\sim$ 260 cm^2 at 100 keV; see Fig. 2.5). The energy resolution is $\sim$ 3.0 keV (FWHM) for the PIN diodes, and $7.6/\sqrt{E}$ % (FWHM) for the scintillators where E is energy in MeV. The HXD time resolution is 61 μs.

7.1 GSO/BGO Counter Units

Each main detector unit is of a well-type design with active anti-coincidence shields. The shields and the coarse collimator itself are made of Bismuth Germanate (BGO; $Bi_4Ge_3O_{12}$) crystals, while the X–ray sensing material "inside the well" is GSO (Gadolinium Silicate, or $Gd_2SiO_5(Ce)$) crystal. The aspect ratio of the coarse collimators yields an acceptance angle for the GSO of 4.5^o (FWHM). Each unit thus forms a 2 $\times$ 2 matrix, containing four 24 mm $\times$ 24 mm, 5 mm thick GSO crystals, each placed behind the PIN diode. The BGO crystals are also placed underneath of the GSO sensors, and thus each well is a five-sided anti-coincidence system. The effective thickness of the BGO active shield is thus about 6 cm for any direction from the PIN and GSO, except to the pointing direction.

The reason for the choice of the two different crystals for the sensor and the shield is dictated by the large stopping ability of both, yet the very different rise/decay times, of $\sim$ 706 ns for BGO, and $\sim$ 122 ns for GSO, at a working temperature of -20^oC. This allows for an easy discrimination of the shield vs. X–ray sensor signals, where a single PM tube can discriminate between the two types of scintillators in which an event may have occurred. Any particle events or Compton events

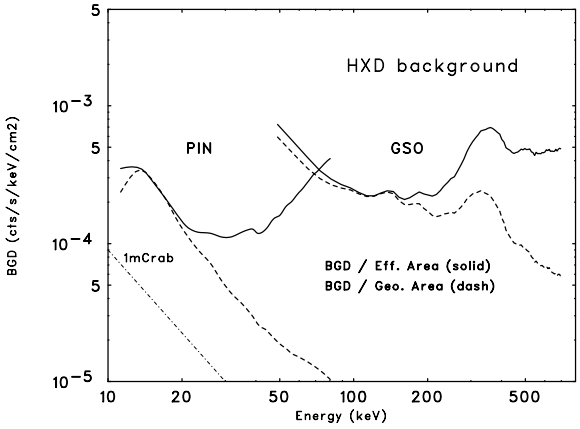

Figure 7.3: Example of the observed HXD background on orbit. Plots normalized both with effective (solid) and geometric (dashed) area are presented.

that are registered by both the BGO and GSO can be rejected by this phoswich technique, utilizing custom-made pulse-shaping LSI circuits.

7.2 PIN Diodes

The low energy response of the HXD is provided by 2 mm thick PIN silicon diodes, placed in front of each GSO crystal. The diodes absorb X–rays with energies below ~ 60 keV, but gradually become transparent to harder X–rays, which in turn reach and are registered by the GSO detectors. The X–rays are photoelectrically absorbed in the PIN diodes, and the signal is amplified, converted to a digital form, and read out by the associated electronics. The PIN diodes are of course also shielded from particle events by the BGO shields, as they are placed inside the deep BGO wells. The four PIN diodes and the PM tube comprises one unit in view of the signal processing.

7.3 HXD field of view

The field of view of the HXD changes with incoming energy. Below ~ 100 keV, the passive fine collimators define a $34' \times 34'$ FWHM square opening. The narrow field of view compared to Beppo-SAX-PDS and RXTE-HEXTE experiments is one of the key issues with HXD observations. Above ~ 100 keV, the fine collimators become transparent and the BGO active collimator defines a $4.5^{o} \times 4.5\ ^{o}$ FWHM square opening. In summary, all the PIN energy range and the lower quarter of the GSO range has a field of view of $34'$, while the GSO events above ~ 100 keV have wider field of view, up to 4.5^{o}.

7.4 HXD Background and Sensitivity

Although the HXD is a non-imaging instrument, its instantaneous background can be reproduced through modeling, without requiring separate off-source observations. The HXD has been designed to achieve an extremely low in-orbit background ($\sim 10^{-4}$ c s^{-1} cm^{-2} keV^{-1}), based on a combination of novel techniques: (1) the five-sided tight BGO shielding as mentioned above; (2) the use of the 20 shielding counters made of thick BGO crystals which surround the 16 main GSO/BGO counters; (3) sophisticated onboard signal processing and onboard event selection, employing both

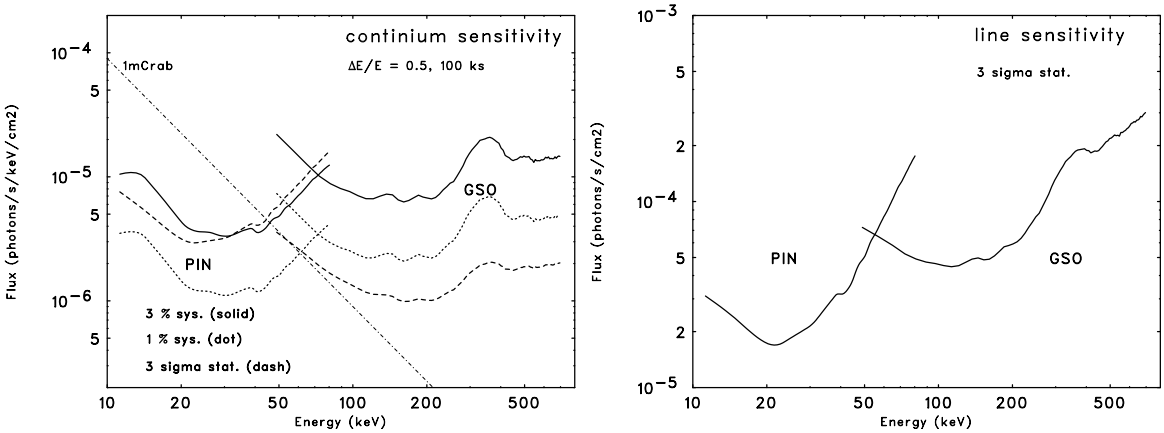

Figure 7.4: [Left] The sensitivity of the HXD to continuum emission, taking into account the expected background. [Right] Same, for line emission.

high-speed parallel hardware circuits in the Analog Electronics, and CPU-based signal handling in the Digital Electronics; and (4) the careful choice of materials that do not become strongly radio-activated under in-orbit particle bombardment. Finally, (5) the narrow field of view below $\sim$ 100 keV defined by the fine collimator effectively reduces both the CXB contribution and the source confusion.

The HXD detector background measured in orbit is plotted in Fig. 7.3. Figure 7.4 [Left] illustrates the sensitivity of the detector for the measurement of the continuum, while Fig. 7.4 [Right] gives the sensitivity to line emission. The HXD background is currently known to correlate with cut-off-rigidity and time-after-SAA, and at least in the GSO band a small growing effect due to radio isotope buildup is detected. In modeling the background, all these effects must be taken into account. As is the case for every non-imaging instrument (and in particular, for those sensitive in the hard X-ray range), the limiting factor for the sensitivity of the HXD will be the error in estimation of background. For one-day averaged background, current (Oct. 2005) estimates of this error are about 5% (at 90 % confidence) for the PIN and about 10% for the GSO. Because the background estimation is in some sense a difficult science, the modeling accuracy will be supported on "best effort" basis. Since this is the first space flight of the HXD-type detector, the details will depend on the experience with in-orbit data, and the status of background estimation error and procedures for background subtraction will be presented on the *Suzaku* websites listed in Appendix C. The background estimation systematics are expected to be less than 3% and 5% within a year for the PIN and the GSO, respectively. The final goal is to achieve 1% and 3%, respectively.

For sources fainter than the background estimation error, background subtraction has to be performed carefully. Typical source flux level to be handled with care, based on current understandings of background estimation error, is listed in table 7.1. In general, for analysis in the energy range up to 40 keV, $\sim$ 1 mCrab is the level to take special care, and for those up to 150 keV, it is $\sim$ 100 mCrab. Above 200 keV, any observation will be strongly affected by background and how it is understood. Please refer to the website at Appendix C for updated information.

7.5 Data analysis procedure

HXD data are accumulated by event by event basis. After on-board data selection, event data are further screened by the ground pipe-line analysis process. By referring to the trigger and flag information (including the inter-unit anti-coincidence hit patterns), the pipe-line assigns specific

Table 7.1: Typical limiting source flux due to the background estimation error.

sys. err	10-30 keV	30-90 keV	90-270 keV	270-600 keV
5%	8*	80	480	4800
3%	5	48	300	3000
1%	1.6	16	100	1000

*flux in 10^{-12} erg s^{-1} cm^{-2}.

Below 100 keV, 1 mCrab is $\sim 16 \times 10^{-12}$ erg s^{-1} cm^{-2} for a band width of a factor of 3.

grades to the HXD events such as pure PIN events and pure GSO events. Detector responses and background files that match the particular grade of the events will be provided by the HXD team. With progress of background modeling, these background files will be updated for all existing observations to date. Note that currently there are no user-specified parameters for the HXD.

7.6 The Anti-coincidence counters as a Wide-band All-sky Monitor (WAM)

Tight active shielding of HXD results in a large arrays of guard counters surrounding the main detector parts. These anti coincidence counters, made of ~ 4 cm thick BGO crystals, have a large effective area for sub-MeV to MeV gamma-rays. With limited angular ($\sim 5^o$) and energy ($\sim 30\%$ at 662 keV) resolutions, they works as a Wide-band All-sky Monitor (WAM).

Analog signals from normally four counters in each side of HXD sensor are summed up and a pulse height histogram is recorded each second. If a transient event such as gamma-ray burst (GRB) is detected, four energy band light curve with finer (31.25 ms) timing resolution is also recorded. The energy coverage of WAM is from ~ 50 keV to ~ 5 MeV, and its effective area is ~ 800 cm^2 at 100 keV and 400 cm^2 at 1 MeV. These data are shared with PI and the HXD team; the PI can utilize the full set of WAM data. Because these transient events, especially GRBs, need spontaneous contribution to the community, the HXD team will make the analysis products, such as light curves and spectra, public as soon as possible.

Appendix A

Acronyms

The following table lists acronyms used in this document.

Acronym	Definition
AAVSO	American Association of Variable Stars Observers
AE	Analog Electronics
AO	Announcement of Opportunity
AGN	Active Galactic Nuclei
ARF	Ancillary Response File
ASCA	Advanced Satellite for Cosmology and Astrophysics
ASM	All-Sky Monitor (on *RXTE*)
BGD	Background
BGO	Bismuth Germanate
BI	Back-Illuminated
CALDB	Calibration Database
CCD	Charge-Coupled Device
Co-I	Co-investigator
CPU	Central Processing Unit
CTE	Charge Transfer Efficiency
CTI	Charge Transfer Inefficiency
CXB	Cosmic X–ray Background
DDT	Director Discretionary Time
DE	Digital Electronics
Dec	Declination
DP	Data Processor
DSN	Deep Space Network
EA	Effective Area
EEF	Encircled Energy Function
EOB	Extensible Optical Bench
EPIC	European Photon Imaging Camera (on *XMM-Newton*)
ESA	European Space Agency
FI	Front-Illuminated
FWHM	Full-Width Half-Maximum
FITS	Flexible Image Transport System
FOV	Field Of View
FSA	Frame Store Area
FTOOLS	FITS Tools

Acronym	Definition
GO	Guest Observer
GOF	Guest Observer Facility
GRB	Gamma-Ray Burst
GSFC	Goddard Space Flight Center
GSO	Gadolinium Silicate
HEASARC	High Energy Astrophysics Science Archive Research Center
HESS	High Energy Stereoscopic System
HETG	High Energy Transmission Grating (on *Chandra*)
HEXTE	High Energy X-ray Timing Experiment (on *RXTE*)
HPD	Half-Power Diameter
HRI	High Resolution Imager (on *ROSAT*)
HV	High Voltage
HXD	Hard X–Ray Detector
ISAS	Institute of Space and Astronautical Science
INTEGRAL	INTErnational Gamma-Ray Astrophysics Laboratory
JAXA	Japan Aerospace Exploration Agency
LETG	Low Energy Transmission Grating (on *Chandra*)
LSI	Large Scale Integration
MIT	Massachusetts Institute of Technology
MPU	Main Processing Unit
NRA	NASA Research Announcement
NASA	National Aeronautics and Space Administration
NOI	Notice Of Intent
NSPIRES	NASA Solicitation and Proposal Integrated Review and Evaluation System
NXB	Non-X–ray Background
OBF	Optical Blocking Filter
PDS	Phoswich Detector System (on *Bepppo-SAX*)
PH	Pulse Height
PIN	Positive Intrinsic Negative
PI	Principal Investigator
PI	Pulse Invariant
PIMMS	Portable Interactive Multi-Mission Simulator
PM	Photo-Multiplier
PPU	Pixel Processing Unit
PSF	Point Spread Function
PSPC	Position-Sensitive Proportional Counter (on *ROSAT*)
P-Sum	Parallel-Sum
QDE	Quantum Detection Efficiency
RA	Right Ascension
RAM	Random Access Memory
RDD	Residual Dark-current Distribution
RGS	Reflection Grating Spectrometer (on *XMM-Newton*)
RFA	Research Focus Area
RMF	Redistribution Matrix File
ROSAT	RÖntgen SATellite
RPS	Remote Proposal Submission
RXTE	Rossi X-ray Timing Explorer
SAA	South Atlantic Anomaly

Acronym	Definition
SAX	Satellite per Astronomia X
S/C	Spacecraft
SGR	Soft Gamma-ray Repeater
SLAC	Stanford Linear Accelerator Center
SMC	Small Magellanic Cloud
SN	SuperNova
SWG	Science Working Group
TBD	To Be Determined
TCE	TEC Control Electronics
TCU	Thermal Control Unit
TEC	Thermo-Electric Cooler
TOO	Target Of Opportunity
US	United States
USC	Uchinoura Space Center
UV	Ultra Violet
VHS	Very High State
VSNET	Variable Star NETwork
WAM	Wide-band All-sky Monitor
XIS	X–Ray Imaging Spectrometer
XRB	X-ray Binary
XRS	X–Ray Spectrometer
XRT	X–Ray Telescope
XRT-I	X–Ray Telescope for one of the four XIS detectors

Appendix B

SWG Target List

The SWG target list is presented here twice, sorted both by type of source and by Right Ascension (RA) and Declination (Dec). Details of targets with constraints are listed in the last section. The details of data processing and filtering are still incomplete, so the total time listed for each observation that is already complete is an only an estimate of the actual good time available.

Data from selected sources will be released before the AO is due. The exact list of sources and times to be released has not been finalized; please check the *Suzaku* website listed in Appendix C for more information.

B.1 Targets Sorted by Category

B.1.1 Calibration

Target	RA	Dec	Stat	Exp.	#obs	Remarks
E0102-72	01 04 02.4	-72 01 60.0	Obs	75	2	XIS window open
E0102-72	01 04 02.4	-72 01 60.0		20	1	XIS
N132D	05 25 03.3	-69 38 27.2	Obs	105	6	HXD HV ON
Crab	05 34 32.0	+22 00 52.2	Obs	170	31	
Eta Carina	10 45 03.6	-59 41 04.3		20	1	XIS
Lockman Hole	10 52 00.0	+57 18 00.0		100	1	HXD
North Ecliptic Pole	18 11 12.0	+66 00 0.0	Obs	70	1	
Vega	18 36 56.3	+38 47 01.3	Obs	10	1	Optical light leak check
PKS2155-304	21 58 52.1	-30 13 32.1		60	1	XIS; coordinated obs. with XMM-Newton
Cas A	23 23 24.0	+58 48 54.0		10	1	XIS

B.1.2 Gamma-Ray Burst

Target	RA	Dec	Pri.	Exp.	#obs	Remark
GRB AFTERGLOW	00 00 00.0	+00 00 00.0	A(TOO)	150	TBD	

B.1.3 Galactic Compact Objects

Target	RA	Dec	Stat	Exp	#obs	Remark
73P/SW3	01 24 08.4	-10 09 02.		35	2	Constrained, May 2006
AB Dor	05 28 44.7	-65 26 56.0	Obs	5	1	
Eta Carina	10 45 03.6	-59 41 04.2	Obs	35	1	
PSR1509-58	15 13 56.1	-59 08 08.2	Obs	50	1	
X1543-475	15 47 08.6	-47 40 09.		200	10	Constrained TOO in outburst (ASM) one of seven
XTE J1550-564	15 50 58.8	-56 28 35.0		40	1	TOO, VHS of one of two sources
XTE J1550-564	15 50 58.8	-56 28 35.0		200	10	Constrained TOO in outburst (ASM) one of seven
4U1626-67	16 32 16.8	-67 27 42.8	Obs	5	1	
4U1626-67	16 32 16.8	-67 27 43.		100	1	
X1630-472	16 34 01.1	-47 23 34.4		200	10	Constrained TOO in outburst (ASM) one of seven
GRO J1655-40	16 54 00.0	-39 50 44.		40	1	TOO, VHS of one of two sources
Her X-1	16 57 49.8	+35 20 32.6	Obs	30	1	
XTE J1650-500	16 50 01.0	-49 57 45.0		200	10	Constrained TOO in outburst (ASM) one of seven
GRO J1655-40	16 54 0.0	-39 50 42.0	Obs	35	1	
GRO J1655-40	16 54 00.0	-39 50 44.9		200	10	Constrained TOO in outburst (ASM) one of seven
GX 339-4	17 02 49.4	-48 47 22.6		200	10	Constrained TOO in outburst (ASM) one of seven
GX 349+2	17 05 44.5	-36 25 23.		50	1	
RXJ BGD2	17 09 05.0	-41 02 06.0	Obs	30	1	
RXJ BGD1	17 09 31.9	-38 49 22.8	Obs	30	1	
RXJ 1713-3946	17 12 17.0	-39 56 09.6	Obs	60	1	
GX17+2	18 16 01.4	-14 02 09.6	Obs	5	1	
AM Her	18 16 13.3	+49 52 04.8	Obs	10	1	
V4641 SGR	18 19 21.6	-25 24 25.		100	1	TOO, in outburst (VSNET/ASM)
XTE J1859+226	18 58 41.5	+22 39 29.9		200	10	Constrained TOO in outburst (ASM) one of seven
GRS1915+105	19 15 11.6	+10 56 44.2	Obs	80	1	
CH CYG	19 24 13.9	+50 10 11.		60	1	
Cyg X-1	19 58 21.8	+35 12 06.5	Obs	15	1	
73P/SW3	20 26 48.8	+29 44 27.		5	1	Constrained, May 2006
AE AQUARII	20 40 09.2	-00 52 15.		100	1	
73P/SW3	21 20 37.0	+24 41 28.		20	3	Constrained, May 2006
SS CYG	21 42 42.7	+43 35 09.		40	1	
SS CYG	21 42 42.7	+43 35 09.		60	1	TOO, in outburst (AAVSO)

B.1.4 Galactic Diffuse Emission

Target	RA	Dec	Stat	Exp	#obs	Remark
Tycho center	00 25 20.4	+64 08 16.		100	1	
Tycho offset	00 47 00.0	+65 30 00.		50	1	
SMC DIFFUSE 1	00 52 09.6	-72 49 48.		50	1	
E0102-72	01 04 02.4	-72 01 59.9	Obs	25	1	
MBM12	02 55 50.0	+19 30 10.		100	1	
DEM L71/N23	05 05 46.4	-67 56 43.1	Obs	40	1	
N103B	05 08 54.3	-68 44 17.9	Obs	35	1	
SN 1987A	05 35 28.0	-69 16 11.		40	1	
A0535+26	05 38 54.5	26 18 57.6	Obs	20	1	
RXJ 0852-4622 NW	08 48 58.0	-45 39 03		200	1	
HESS J1616-508-BGD	16 14 38.8	-51 10 34.7	Obs	20	1	
HESS J1616-508	16 16 29.0	-50 53 58.2	Obs	45	1	
HESS J1616-508-BGD2	16 17 50.9	-50 41 27.6	Obs	20	1	
RCW86 SW	14 41 08.6	-62 40 25.		100	1	
SN1006 SW-BG	14 58 36.0	-42 24 00.0	Obs	35	1	
SN1006 SW-rim	15 02 00.0	-42 4 12.0	Obs	50	1	
SN1006 NW	15 02 33.6	-41 48 00.		50	1	
SN1006 SE	15 03 28.8	-42 04 48.		50	1	
SN1006 NE-rim	15 03 50.4	-41 46 48.0	Obs	50	1	
SN1006 NE-BG	15 06 48.0	-41 24 00.0	Obs	50	1	
Galactic Bulge	15 45 43.2	-31 41 59.3	Obs	60	1	
North Polar Spur	17 22 21.0	+ 4 45 23.8	Obs	35	1	
Sgr C	17 44 37.3	-29 28 10.		100	1	
Gal Center Bgd2	17 44 49.0	-29 21 07.2	Obs	10	2	
Sgr C Bgd	17 44 56.2	-29 45 52.		10	1	
Gal Center Src2	17 45 12.7	-29 10 15.6	Obs	75	2	
Gal Center Src1	17 46 02.6	-28 55 33.6	Obs	70	2	
Gal Center Bgd1	17 46 05.5	-29 30 54.0	Obs	10	2	
Gal Center Bgd1	17 46 05.5	-29 30 54.0	Obs	5	1	
Gal Center Bgd3	17 46 21.6	-28 39 03.6	Obs	10	2	
Galactic Center 2	17 47 05.4	-28 37 52.		100	1	
Sgr B2	17 47 30.1	-28 26 27.2	Obs	60	1	
GC Sgr B2 Bgd	17 48 22.2	-28 07 58.8	Obs	10	1	
Galactic Bulge 2	18 02 29.0	-29 35 10.		10	1	
HESS J1804-216 BG	18 03 50.4	-22 01 27.		50	1	
HESS J1804-216	18 04 41.1	-21 40 33.		50	1	
Galactic Bulge 3	18 18 50.0	-31 29 09.		50	1	
Galactic Ridge	18 44 00.0	-04 04 12.		100	1	
Galactic Bulge 6	18 50 45.0	-33 53 34.		10	1	
BD+30.3639	19 34 45.1	30 30 57.6	Obs	30	1	
Cyg Loop	20 53 57.5	+32 22 24.		20	1	Roll constrained
Cyg Loop	20 54 59.1	+32 11 17.		20	1	Roll constrained
Cyg Loop	20 55 49.2	+31 57 39.		20	1	Roll constrained
Cyg Loop	20 56 42.3	+31 44 43.		20	1	Roll constrained
Cas A	23 23 24.0	58 48 54.0	Obs	20	1	

B.1.5 Extragalactic Compact Sources

Target	RA	Dec	Stat	Exp	#obs	Remark
GRB TOO	00 00 00.0	+00 00 00.		150	3	
NGC 1313 ULX	03 18 15.4	-66 31 59.9	Obs	40	1	
3C120	04 33 11.1	+05 21 15.		160	4	
NGC 2110	05 52 11.4	-07 27 22.0	Obs	85	1	
1H 0707-495	07 08 41.5	-49 33 06.		100	1	
SWIFT J0746.3+254	07 46 25.9	+25 49 02.		100	1	
0836+714	08 41 24.3	+70 53 41.		50	1	
NGC 2992	09 45 42.1	-14 19 35.		120	3	Constrained
MCG-5-23-16	09 47 40.1	-30 56 56.		100	1	
1ES1101-232	11 03 37.6	-23 29 30.		80	1	HESS TOO, 2 of 6
MRK 421	11 04 27.3	+38 12 31.		80	1	HESS TOO, 2 of 6
NGC 3516	11 06 47.5	+72 34 07.0	Obs	100	1	
NGC 4051	12 03 09.6	+44 31 53.		150	1	
PG 1211+143	12 14 17.7	+14 03 13.		100	1	
NGC 4945	13 05 27.5	-49 28 05.5	Obs	15	1	
NGC 4945	13 05 27.5	-49 28 05.5	Obs	15	1	
Cen A	13 25 27.6	-43 01 08.8	Obs	40	1	
MCG-6-30-15	13 35 53.8	-34 17 44.		300	4	
MCG-6-30-15	13 35 54.0	-34 17 42.4	Obs	50	1	
ARP220	15 34 57.1	+23 30 11.		100	1	
Mkn 501	16 53 52.2	+39 45 37		80	1	HESS TOO, 2 of 6
QSO1727+5	17 28 18.3	+50 13 09.8	Obs	3	1	
PKS 2005-489	20 09 25.4	-48 49 53.		80	1	HESS TOO, 2 of 6
PKS2155-304	21 58 52.1	-30 13 32.		80	1	HESS TOO, 2 of 6
H 2356-309	23 59 07.8	-30 37 37.		80	1	HESS TOO, 2 of 6

B.1.6 Extragalactic Diffuse Sources

Target	RA	Dec	Stat	Exp	#obs	Remark
ABELL2801	00 38 31.3	-29 02 47.		25	1	
ABELL2804	00 39 38.7	-28 53 21.		25	1	
ABELL2811-OFF	00 40 54.0	-28 42 57.		25	1	
ABELL2811	00 42 09.3	-28 32 33.		25	1	
NGC 720	01 53 00.5	-13 44 19.		100	1	
A426	03 19 48.1	+41 30 42.		50	1	
Fornax Cluster	03 38 34.6	-35 29 07.8	Obs	50	1	
Fornax Cluster NO	03 38 34.6	-35 14 07.		80	1	
A3376 WEST RELIC	06 00 00.0	-40 02 00.		150	1	
ABELL 3376	06 02 15.0	-39 57 00.0	Obs	130	1	
NGC 2403	07 36 51.4	+65 36 09		70	1	
M82 Wind	09 55 28.5	+69 45 19.4	Obs	20	1	
A1060	10 36 24.0	-27 31 35.		40	1	
A1060 OFFSET	10 37 45.0	-27 31 35.		60	1	
A1413	11 55 18.9	+23 38 31.		100	1	
NGC 4388	12 25 46.9	+12 39 43.		100	1	
NGC 4636	12 42 54.0	+02 45 07.		80	1	
CENTAURUS CLUSTER	12 48 49.3	-41 18 40.		30	1	
CENCL OFFSET1	12 48 49.3	-41 26 38.		40	1	
CENCL OFFSET2	12 48 49.3	-41 10 40.		40	1	
HCG62	12 53 06.0	-09 12 15.		100	1	
ABELL 1795	13 48 52.6	+26 35 31.		120	1	
A2052	15 16 45.5	+07 00 01.1	Obs	15	1	$(+7',+7')$
A2052	15 16 45.5	+07 00 01.1	Obs	20	1	$(-7',+7')$
A2052	15 16 45.5	+07 00 01.1	Obs	10	1	$(-7',-7')$
A2052	15 16 45.5	+07 00 01.1	Obs	15	1	$(+7',-7')$
A2218 offset	16 17 48.0	+65 27 36.0	Obs	35	1	
A2218	16 35 54.2	+66 12 59.8	Obs	35	1	
A2218 offset B	16 39 30.8	+65 13 31.2		50	1	
A2312	18 53 48.2	+68 23 06.0	Obs	4	1	

B.2 Targets Sorted by RA

Abbrev.	Target Type
GRB	Gamma-Ray Burst
CAL	Calibration
GDE	Galactic Diffuse Emission
GCS	Galactic Compact Sources
EDS	Extragalactic Diffuse Sources
ECS	Extragalactic Compact Sources

Target	RA	Dec	Cat	Stat	Exp.	#obs
GRB AFTERGLOW	00 00 00.0	+00 00 00.0	GRB		150	3
ABELL2811	00 42 09.3	-28 32 33.	EDS		25	1
ABELL2811-OFF	00 40 54.0	-28 42 57.	EDS		25	1
ABELL2804	00 39 38.7	-28 53 21.	EDS		25	1
ABELL2801	00 38 31.3	-29 02 47.	EDS		25	1
Tycho center	00 25 20.4	+64 08 16.	GDE		100	1
Tycho offset	00 47 00.0	+65 30 00.	GDE		50	1
SMC DIFFUSE 1	00 52 09.6	-72 49 48.	GDE		50	1
E0102-72	01 04 02.4	-72 01 60.0	CAL	Obs	75	2
E0102-72	01 04 02.4	-72 01 60.0	CAL		20	1
E0102-72	01 04 02.4	-72 01 60.0	GDE	Obs	25	1
73P/SW3	01 24 08.4	-10 09 02.	GCS		35	2
NGC720	01 53 00.5	-13 44 19.	EDS		100	1
MBM12	02 55 50.0	+19 30 10.	GDE		100	1
NGC 1313 ULX	03 18 15.4	-66 31 59.9	ECS	Obs	40	1
A426	03 19 48.1	+41 30 42.	EDS		50	1
Fornax Cluster	03 38 34.6	-35 29 07.8	EDS	Obs	50	1
FORNAX CLUSTER NO	03 38 34.6	-35 14 07.	EDS		80	1
3C120	04 33 11.1	+05 21 15.	ECS		160	4
DEM L71/N23	05 05 46.4	-67 56 43.1	GDE	Obs	40	1
N103B	05 08 54.3	-68 44 17.9	GDE	Obs	35	1
N132D	05 25 03.3	-69 38 27.2	CAL	Obs	105	6
AB Dor	05 28 44.7	-65 26 56.0	GCS	Obs	5	1
Crab	05 34 32.0	+22 00 52.2	CAL	Obs	170	31
SN 1987A	05 35 28.0	-69 16 11.	GDE		40	1
A0535+26	05 38 54.5	26 18 57.6	GDE	Obs	20	1
NGC 2110	05 52 11.4	-07 27 22.0	ECS	Obs	85	1
A3376 WEST RELIC	06 00 00.0	-40 02 00.	EDS		150	1
ABELL 3376	06 02 15.0	-39 57 00.0	EDS	Obs	130	1

Target	RA	Dec	Cat	Stat	Exp.	#obs
1H 0707-495	07 08 41.5	-49 33 06.	ECS		100	1
NGC 2403	07 36 51.4	+65 36 09		70	1	
SWIFT J0746.3+254	07 46 25.9	+25 49 02.	ECS		100	1
0836+714	08 41 24.3	+70 53 41.	ECS		50	1
RXJ 0852-4622 NW	08 48 58.0	-45 39 03	GDE		200	1
NGC 2992	09 45 42.1	-14 19 35.	ECS		120	3
MCG-5-23-16	09 47 40.1	-30 56 56.	ECS		100	1
M82 Wind	09 55 28.5	+69 45 19.4	EDS	Obs	20	1
Eta Carina	10 45 03.6	-59 41 04.3	CAL		20	1
Eta Carina	10 45 03.6	-59 41 04.3	GCS	Obs	35	1
Lockman Hole	10 52 00.0	+57 18 00.0	CAL		100	1
A1060	10 36 24.0	-27 31 35.	EDS		40	1
A1060 OFFSET	10 37 45.0	-27 31 35.	EDS		60	1
1ES1101-232	11 03 37.6	-23 29 30.	ECS		80	1 (TOO,2/6)
MRK 421	11 04 27.3	+38 12 31.	ECS		80	1 (TOO,2/6)
NGC 3516	11 06 47.5	+72 34 07.0	ECS	Obs	100	1
A1413	11 55 18.9	+23 38 31.	EDS		100	1
NGC 4051	12 03 09.6	+44 31 53.	ECS		150	1
PG 1211+143	12 14 17.7	+14 03 13.	ECS		100	1
NGC4388	12 25 46.9	+12 39 43.	EDS		100	1
NGC4636	12 42 54.0	+02 45 07.	EDS		80	1
CENTAURUS CLUSTER	12 48 49.3	-41 18 40.	EDS		30	1
CENCL OFFSET1	12 48 49.3	-41 26 38.	EDS		40	1
CENCL OFFSET2	12 48 49.3	-41 10 40.	EDS		40	1
HCG62	12 53 06.0	-09 12 15.	EDS		100	1
Cen A	13 25 27.6	-43 1 08.8	ECS	Obs	40	1
NGC 4945	13 05 27.5	-49 28 05.5	ECS	Obs	15	1
NGC 4945	13 05 27.5	-49 28 05.5	ECS	Obs	15	1
MCG-6-30-15	13 35 53.8	-34 17 44.	ECS		300	4
MCG-6-30-15	13 35 54.0	-34 17 42.4	ECS	Obs	50	1
ABELL 1795	13 48 52.6	+26 35 31.	EDS		120	1
RCW86 SW	14 41 08.6	-62 40 25.	GDE		100	1
SN1006 SW-BG	14 58 36.0	-42 24 00.0	GDE	Obs	35	1
SN1006 SW-rim	15 02 00.0	-42 4 12.0	GDE	Obs	50	1
SN1006 NW	15 02 33.6	-41 48 00.	GDE		50	1
SN1006 SE	15 03 28.8	-42 04 48.	GDE		50	1
SN1006 NE-rim	15 03 50.4	-41 46 48.0	GDE	Obs	50	1
SN1006 NE-BG	15 06 48.0	-41 24 00.0	GDE	Obs	50	1
PSR1509-58	15 13 56.1	-59 08 08.2	GCS	Obs	50	1
A2052	15 16 45.5	+07 00 01.1	EDS	Obs	15	1
A2052	15 16 45.5	+07 00 01.1	EDS	Obs	20	1
A2052	15 16 45.5	+07 00 01.1	EDS	Obs	10	1
A2052	15 16 45.5	+07 00 01.1	EDS	Obs	15	1
ARP220	15 34 57.1	+23 30 11.	ECS		100	1
Galactic Bulge	15 45 43.2	-31 41 59.3	GDE	Obs	60	1
X1543-475	15 47 08.6	-47 40 09.	GCS		200	10 (TOO,1/7)
XTE J1550-564	15 50 58.8	-56 28 35.0	GCS		200	10 (TOO,1/7)
XTE J1550-564	15 50 58.8	-56 28 35.0	GCS		40	1 (TOO,1/2)

Target	RA	Dec	Cat	Stat	Exp.	#obs
HS J1616-508-BGD	16 14 38.8	-51 10 34.7	GDE	Obs	20	1
HESS J1616-508	16 16 29.0	-50 53 58.2	GDE	Obs	45	1
A2218 offset	16 17 48.0	+65 27 36.0	EDS	Obs	35	1
A2218 offset B	16 39 30.8	+63 13 31.2	EDS		50	1
HS J1616-508-BGD2	16 17 50.9	-50 41 27.6	GDE	Obs	20	1
4U1626-67	16 32 16.8	-67 27 43.	GCS		100	1
4U1626-67	16 32 16.8	-67 27 42.8	GCS	Obs	5	1
X1630-472	16 34 01.1	-47 23 34.4	GCS		200	10 (TOO,1/7)
A2218	16 35 54.2	+66 12 59.8	EDS	Obs	85.9	1
XTE J1650-500	16 50 01.0	-49 57 45.0	GCS		200	10 (TOO,1/7)
Mkn 501	16 53 52.2	+39 45 37	ECS		80	1 (TOO,2/6)
GRO J1655-40	16 54 00.0	-39 50 44.	GCS		40	1 (TOO,1/2)
GRO J1655-40	16 54 00.0	-39 50 44.9	GCS		200	10 (TOO,1/7)
GRO J1655-40	16 54 00.0	-39 50 42.0	GCS	Obs	35	1
Her X-1	16 57 49.8	+35 20 32.6	GCS	Obs	30	1
GX 339-4	17 02 49.4	-48 47 22.6	GCS		200	10 (TOO,1/7)
GX 349+2	17 05 44.5	-36 25 23.	GCS		50	1
RXJ BGD2	17 09 05.0	-41 02 06.0	GCS	Obs	30	1
RXJ BGD1	17 09 31.9	-38 49 22.8	GCS	Obs	30	1
RXJ 1713-3946	17 12 17.0	-39 56 09.6	GCS	Obs	60	1
North Polar Spur	17 22 21.0	+04 45 23.8	GDE	Obs	35	1
QSO1727+5	17 28 18.3	+50 13 09.8	ECS	Obs	3	1
Sgr C	17 44 37.3	-29 28 10.	GDE		100	1
Gal Center Bgd2	17 44 49.0	-29 21 07.2	GDE	Obs	10	2
Sgr C Bgd	17 44 56.2	-29 45 52.	GDE		10	1
Gal Center Src2	17 45 12.7	-29 10 15.6	GDE	Obs	75	2
Gal Center Src1	17 46 02.6	-28 55 33.6	GDE	Obs	70	2
Gal Center Bgd1	17 46 05.5	-29 30 54.0	GDE	Obs	10	2
Gal Center Bgd3	17 46 21.6	-28 39 03.6	GDE	Obs	10	2
Galactic Center 2	17 47 05.4	-28 37 52.	GDE		100	1
Sgr B2	17 47 30.1	-28 26 27.2	GDE	Obs	60	1
GC Sgr B2 Bgd	17 48 22.2	-28 07 58.8	GDE	Obs	10	1
N. Ecliptic Pole	18 11 12.0	+66 00 00.0	CAL	Obs	70	1
GX17+2	18 16 01.4	-14 02 09.6	GCS	Obs	5	1
AM Her	18 16 13.3	+49 52 04.8	GCS	Obs	10	1
V4641 SGR	18 19 21.6	-25 24 25.	GCS		100	1 (TOO)
Vega	18 36 56.3	+38 47 01.3	CAL	Obs	10	1
A2312	18 53 48.2	+68 23 06.0	EDS	Obs	4	1
Galactic Bulge 2	18 02 29.0	-29 35 10.	GDE		10	1
HESS J1804-216 BG	18 03 50.4	-22 01 27.	GDE		50	1
HESS J1804-216	18 04 41.1	-21 40 33.	GDE		50	1
Galactic Bulge 3	18 18 50.0	-31 29 09.	GDE		50	1
Galactic Ridge	18 44 00.0	-04 04 12.	GDE		100	1
Galactic Bulge 6	18 50 45.0	-33 53 34.	GDE		10	1
XTE J1859+226	18 58 41.5	+22 39 29.9	GCS		200	10 (TOO,1/7)
GRS1915+105	19 15 11.6	+10 56 44.2	GCS	Obs	80	1
CH CYG	19 24 13.9	+50 10 11.	GCS		60	1
BD+30.3639	19 34 45.1	30 30 57.6	GDE	Obs	30	1
Cyg X-1	19 58 21.8	+35 12 06.5	GCS	Obs	15	1

Target	RA	Dec	Cat	Stat	Exp.	#obs
PKS 2005-489	20 09 25.4	-48 49 53.	ECS		80	1 (TOO,2/6)
73P/SW3	20 26 48.8	+29 44 27.	GCS		5	1
AE AQUARII	20 40 09.2	-00 52 15.	GCS		100	1
Cyg Loop	20 53 57.5	+32 22 24.	GDE		20	1
Cyg Loop	20 54 59.1	+32 11 17.	GDE		20	1
Cyg Loop	20 55 49.2	+31 57 39.	GDE		20	1
Cyg Loop	20 56 42.3	+31 44 43.	GDE		20	1
73P/SW3	21 20 37.0	+24 41 28.	GCS		20	3
SS CYG	21 42 42.7	+43 35 09.	GCS		40	1
SS CYG	21 42 42.7	+43 35 09.	GCS		60	1 (TOO)
PKS2155-304	21 58 52.1	-30 13 32.1	CAL		60	1
PKS2155-304	21 58 52.1	-30 13 32.	ECS		80	1 (TOO,2/6)
Cas A	23 23 24.0	+58 48 54.0	CAL		10	1
Cas A	23 23 24.0	58 48 54.0	GDE	Obs	20	1
H 2356-309	23 59 07.8	-30 37 37.	ECS		80	1 (TOO,2/6)

Appendix C

Important Web/e-mail/postal addresses

Primary *Suzaku* Sites

Japan: `http://www.astro.isas.jaxa.jp/suzaku/`

US : `http://suzaku.gsfc.nasa.gov/`

ESA: `http://www.rssd.esa.int/suzaku`

***Suzaku* GOF:**

`http://suzaku.gsfc.nasa.gov/`

The "Proposal & Tools" button is of particular note.

Tools:

Viewing	`http://heasarc.gsfc.nasa.gov/Tools/Viewing.html`
PIMMS	`http://heasarc.gsfc.nasa.gov/docs/software/tools/pimms.html`
MAKI	`http://heasarc.gsfc.nasa.gov/Tools/maki/maki.html`
XSPEC	`http://heasarc.gsfc.nasa.gov/docs/xanadu/xspec/index.html`
WebPIMMS	`http://heasarc.gsfc.nasa.gov/Tools/w3pimms.html`
WebSPEC	`http://heasarc.gsfc.nasa.gov/webspec/webspec.html`

Questions:

The US GOF can be reached using the web form available at the bottom of every page within the Suzaku GOF site.

Technical Description

Japan: `http://www.astro.isas.jaxa.jp/suzaku/research/proposal/ao1/`

US: `http://heasarc.gsfc.nasa.gov/docs/astroe/prop_tools/suzaku_td/`

ESA: `http://www.rssd.esa.int/index.php?project=ASTROE2&page=AODocs`

US (ftp): `ftp://legacy.gsfc.nasa.gov/suzaku/nra_info/suzaku_td.ps.gz`

SWG Target list

Japan: `http://www.astro.isas.jaxa.jp/suzaku/research/accept/swg_lst.html`

US: `http://heasarc.gsfc.nasa.gov/docs/astroe/prop_tools/swg_lst.html`

RPS (for Japanese proposals)

`http://rps.astro.isas.jaxa.jp/cgi-bin/RPS/SUZAKU/RPS.pl`

RPS (for US proposals)

`http://heasarc.gsfc.nasa.gov/cgi-bin/RPS/SUZAKU/RPS.pl`

(or email `rps@legacy.gsfc.nasa.gov`)

RPS (for ESA proposals)

`http://www.rssd.esa.int/cgi-bin/RPS/SUZAKU/RPS.pl`

(Or email `rps@rssd.esa.int`)